University of New Mexico

Dissertation Proposal

Reduced Order Monte Carlo Modeling of Radiation Transport in Random Media

Author:
Aaron Olson

Supervisor:
Dr. Anil Prinja

Submitted in partial fulfillment of the requirements
for the degree of

in the

Doctor of Philosophy in
Engineering

May 2015

Abstract

Uncertainty quantification in engineering problems such as radiation transport calculations has become a topic of interest in recent years. In many cases the uncertainty due to approximations, bias, or a lack of accurate data is simply not known. In other cases methods such as random sampling of uncertain parameters is used to gain insight into the uncertainty in a quantity of interest. For some problems only a few samples are solvable with available computational time. For other problems uncertainty can be resolved, but not on a routine basis. This research seeks to further develop methods which can be used for large-scale uncertainty quantification problems involving a Monte Carlo solve of the radiation transport equation. Two underlying spectral methods are proposed for UQ applications to the one-dimensional, steady-state, mono-energetic, neutral-particle, and isotropically-scattering radiation transport equation when solved using the Monte Carlo method of particle simulation. The first utilizes the polynomial chaos expansion (PCE) through implementations of the stochastic Galerkin method (SGM) and stochastic collocation method (SCM) when applied to uncertainty in spatially discrete material cross sections and utilizing correlated sampling methods in the underlying Monte Carlo solve. Current work has demonstrated the viability of this method but needs to be further quantified and published. Proposed work is to include sparse, anisotropic, and adaptive collocation grids. Another project uses the Karhunen Loève (KL) expansion to represent spatially varying total cross sections including binary statistical media and those which vary according to a Gaussian-random process. The SCM is proposed for use upon the uncertain coefficients which remain after a truncation of the KL expansion, limiting the number of required transport solves. The resulting spatially-continuously varying cross sections are to be solved for transport results using the Woodcock Monte Carlo (WMC) method, a solution method devoid of discretization bias. This research seeks to make UQ problems involving Monte Carlo radiation transport more attainable and repeatable and pave the way for further innovation.

Contents

Chapter 1

Intoduction

The radiation transport equation allows for the characterization of a particle flux profile throughout a domain. From the flux profile many other quantities can be derived including energy and charge deposition, displacements in material, fission rates, and more. Solution of the radiation transport equation is useful in medical physics, nuclear energy generation, weapons maintenance and development, nuclear nonproliferation, fusion experiments, and in many other problem types.

Of particular interest for some of these problems is uncertainty analysis about the results of such transport calculations. Two sources of uncertainty in the solution of particle transport problems that are often of interest are uncertainty in nuclear cross sections or uncertainty in material geometry. Understanding uncertainty in quantities of interest in particle transport allows better design and implementation across various fields creating cheaper, safer, and more effective engineering systems.

Uncertainty in nuclear cross sections arises largely since nuclear cross section data is generated experimentally and there has not yet been sufficient time, resources, and in some cases methods to determine the vast array of nuclear cross sections which might be of interest with a high degree of precision. Cross section data is needed for every type of nuclear interaction for each type of radiation particle interacting with each isotope at every particle energy. Many cross sections have been determined with large error bars and others have yet only been approximated with models. The ability to quantify error in particle flux and derived quantities of interest based on given uncertainties or other assumptions about the nuclear cross section data is useful in nearly every type of radiation transport problem including determination of criticality in nuclear reactors or storage facilities, energy deposition in medical physics applications, material degradation in electrical and mechanical systems operating in radiation environments, and many others.

Uncertainty in the geometry of a problem for which the radiation transport equation is solved views nuclear cross sections as a process in physical space. Problems with non-uniform material density or isotopic abundance qualify. The first occurs in situations such as temperature gradients in nuclear reactor coolant and the second occurs in situations such as non-uniform burn-up or nuclear decay across nuclear systems or non-equilibrium diffusion of one fluid in another. A special class of problems involving uncertain geometry involves two materials which mix in physically discrete pockets such that a ray through the mixture experiences the two materials in lengths distributed exponentially. These binary Markov materials occur in applications such as the mixing of plasmas on the edge of a fuel pellet in laser confined fusion during a fusion shot, the mixing of water and air in Boiling Water nuclear reactors, and the mixing of the various discrete components of concrete of particular interest when used as a radiation shielding material. For these problem types producing physical realizations of the geometry through which to effect transport, especially in a way efficient in radiation transport, is of interest.

The work done in preparation for this proposal and proposed in it uses various reduced order models to quantify the error in particle flux and related quantities in radiation transport equations involving uncertain material cross sections and uncertain geometries using the Monte Carlo method of particle simulation to solve the underlying radiation transport equation. In one problem we characterize the uncertainty in particle flux due to the uncertainty in nuclear cross sections through application of the polynomial chaos expansion (PCE). This involves several implementations of the stochastic Galerkin method (SGM) and stochastic collocation method (SCM), each seeking to benefit from unique properties of the Monte Carlo particle simulation approach through moment coupling and correlated sampling. In another problem we model binary Markov materials using the Karhunen-Loève (KL) decomposition, effecting transport through a modified version of the Monte Carlo simulation known as Woodcock Monte Carlo (WMC). Finally we propose to model other cases of uncertain geometry using the KL decomposition, effecting transport with WMC, and increasing the efficiency of the solve through application of the SCM over the random variables of the KL decomposition.

The rest of this dissertation is organized as follows:

- Chapter 2: We mathematically state the random particle transport equation, discuss two of its applications and its solution using random sampling, and present some of the theory of the Karhunen-Loève decomposition and polynomial chaos expansion which will be later utilized.

- Chapter 3: We describe work done by the author in utilizing various applications of the polynomial chaos expansion to characterize uncertainty in flux based upon uncertainty in nuclear cross sections.

- Chapter 4: We describe work done by the author in using the Karhunen-Loéve decomposition to effect transport through binary Markov materials.

- Chapter 5: We describe proposed work in extension of the work in Chapters 2 and 3 and propose use of the KL expansion and WMC to model and effect transport through materials with total cross sections which are Gaussian-derived random processes in physical space.

Chapter 2

Random Transport Problem

2.1 Random Transport Equation

The steady-state, one-dimensional, mono-energetic, isotropically-scattering, neutral-particle stochastic transport equation which we will focus on can be written:

$$\mu \frac{\partial \psi(x,\mu,\omega)}{\partial x} + \Sigma_t(x,\omega)\psi(x,\mu,\omega) = \frac{\Sigma_s(x,\omega)}{2}\int_{-1}^{1} d\mu' \psi(x,\mu',\omega), \tag{2.1a}$$

$$0 \leq x \leq s; \qquad -1 \leq \mu \leq 1 \tag{2.1b}$$

$$\psi(0,\mu,\omega) = 2, \quad \mu > 0; \qquad \psi(s,\mu,\omega) = 0, \quad \mu < 0, \tag{2.1c}$$

where $\mu = cos(\theta)$ is the cosine of the angle of particle travel with respect to the forward direction, ω denotes a stochastic realization, $\Sigma_t(x,\omega)$ and $\Sigma_t(x,\omega)$ are uncertain coefficients representing the total and scattering particle interaction cross sections, and $\psi(x,\mu,\omega)$ is the spatially, angularly, and stochastically dependent response function known as angular particle flux. The spatial domain extends from the "left" boundary of $x = 0$ to the "right" boundary of $x = s$. In one dimensional "slab" geometry direction of particle travel spans $\mu \in [-1, 1]$. The first boundary condition imposes an isotropically distributed source of strength two such that the flux normally incident upon the left boundary has an intensity of one. The second boundary condition imposes a vacuum condition on the right boundary such that no particle flux enters the problem from this domain boundary. Both of the boundary conditions implicitly enforce that any particles traveling out of the domain are lost to the system.

In addition to using the angular particle flux $\psi(\mu, x, \omega)$ as the quantity of interest we at various times are interested in either of two quantities derived from this response function: scalar particle flux $\phi(x, \omega)$ and the particle current $J(x, \omega)$. The scalar flux is the particle flux irrespective of, or integrated over, direction of particle travel

$$\phi(x, \omega) = \int_{-1}^{1} d\mu' \psi(x, \mu', \omega). \tag{2.2}$$

Scalar flux is of interest since many other quantities are independent of the direction of particle travel and can be derived from the scalar flux. Additionally, various approximations and acceleration methods to the particle transport problem take advantage of the reduced dimensionality of the scalar flux. The net particle current is the net flux traveling normally-incident through a surface or:

$$\int_{-1}^{1} d\mu' \mu' \psi(x, \mu', \omega) = J(x, \omega), \tag{2.3}$$

The net current can be split into the normally-incident flux traveling in each direction through a surface:

$$J(x, \omega) = J^{+}(x, \omega) - J^{-}(x, \omega) \tag{2.4}$$

where the superscripts "+" and "−" denote the right and left direction of particle travel. These particle currents are more fully described

$$J^{+}(x, \omega) = \int_{0}^{1} d\mu' \mu' \psi(x, \mu', \omega); \qquad J^{-}(x, \omega) = \left| \int_{-1}^{0} d\mu' \mu' \psi(x, \mu', \omega) \right|. \tag{2.5}$$

An intensity of two is chosen in the first boundary condition in Eq. 2.1c so that incoming particle current on the left boundary is equal to one: $J^{+}(0, \omega) = 1$. The second boundary condition implicitly states that incoming particle current on the right boundary is equal to zero: $J^{-}(s, \omega) = 0$. Formulation of particle current is of additional interest since the currents exiting the slab, slab "transmission" ($J^{+}(s, \omega)$) and "reflection" ($J^{-}(0, \omega)$), are common quantities of interest. Other boundary conditions are common but not used here. An internal source of intensity $\frac{Q(x,\mu)}{2}$ added to Eq. 2.1 is also common.

2.2 Two Types of Random Transport Equations

We investigate two classes of random materials through which we effect transport according to Eq. 2.1. The first class involves random materials with precisely defined geometries involving stochastically varying and spatially discrete random coefficients. This problem type has application whenever nuclear cross sections are not exactly known and is frequently of interest since nuclear cross section data is experimentally determined

and often involves large epistemic and aleatoric uncertainties. The second class involves random geometries. We investigate two types of random geometries, the first in which two materials are mixed randomly according to Markov statistics and the second in which material properties are non-linear transformations of random functions. Binary Markov materials are of interest in applications like photon transport through turbulently mixed materials in laser fusion experiments and clouds and in mixtures of water and air in nuclear reactor applications. Material profiles which are non-linear transformations of random functions can be used to model processes such as the non-uniform burn up in commercial nuclear reactors and mediums which involve spatially varying density.

2.3 Solution of the Random Transport Equation by Random Sampling

Random sampling is the simplest way to solve the random transport equation for either class of problems. In a random sampling approach, many samples of the unknown parameters are taken and the transport equation is solved for quantities of interest for each sample. When solving problems involving random geometry a sample is usually referred to as a realization. The collection of outputs for the quantities of interest is then observed to approximate the true stochastic behavior of each quantity of interest. For example, from the random sample data moments of the quantity of interest can be constructed such as the mean or variance of the ensemble set or probability density functions can be built. This method is reliable and often used as a benchmark for the solution of stochastic problems but converges upon moments of the quantities of interest rather slowly, having a mean convergence of the square root of the number of samples. In order to solve more quickly other methods such as the use of reduced order models investigated in this work are of interest.

The transport equation is often solved for the expectation value of particle flux using either various forms of deterministic solvers such as finite elements methods, or using the Monte Carlo method of particle simulation through random sampling. This research focuses on use of the Monte Carlo method of particle simulation to solve instances of the transport equation, and seeks to benefit from unique properties and applications of this solution method within a reduced order model framework. Though random sampling in uncertain space and the differential equation solution method through random sampling of particle tracks are each appropriately called a Monte Carlo method [1], for clarity we will restrict usage of that title in this work to the second–Monte Carlo sampling of particle tracks–and refer to the first simply as “random sampling”. Two applications

of the Monte Carlo method of particular interest are correlated sampling which allows the solution of more than one similar problem type through correlated random number sequences [2, 3] or with only one set of particle simulations [4, 5] and Woodcock Monte Carlo (WMC) which allows the Monte Carlo solution of transport problems involving spatially continuously varying interaction cross sections [6, 7].

2.4 Reduced Order Models

Reduced order models make a complex problem more quantified and manageable. The first reduced order model we here investigate is the Karhunen-Loève (KL) decomposition, which is the optimal spectral expansion of a second order random process [8, 9]. The KL expansion can be applied to a process if the process covariance is either known or assumed and distributions for the KL random coefficients are either known or assumed. A truncation of the number of terms in the expansion can approximate the process, reducing the randomness in a process to a set of random coefficients. The second reduced order model is that of the polynomial chaos expansion (PCE) which models a process as an expansion of random, orthogonal polynomials. A truncation of the expansion allows for a finite problem. Applying the PCE to a system response function and through polynomial orthogonality, polynomial recursion relationships, and a closure creating a finite system of coupled equations which can be solved for the PCE coefficients is known as the stochastic Galerkin method (SGM). Applying the PCE to a system response function and through polynomial orthogonality and application of quadrature over resulting integrals in order to solve the PCE coefficients is known as the stochastic collocation method (SCM). There are at least two major classifications of the stochastic collocation method in literature, one based on Lagrange interpolating polynomials which developed during the late nineties [10] and another based on Askey polynomials utilized in a PCE introduced in 2003 [11]. Several works acknowledge and compare these two versions of SCM which fundamentally differ through basis polynomials [12–16]. The first, which we will call Lagrangian-based-SCM is probably somewhat more common in literature, but we will use the second which we will simply call SCM through it goes by names such as SCM, PCE-SCM, Non-Intrusive Spectral Projection (NISP), or non-intrusive generalized polynomial chaos. The KL expansion of a process is generally preferred, but requires knowledge of the process covariance function, whereas the PCE does not. The theory of each reduced order model is discussed further here.

2.4.1 Karhunen-Loève Modeling of Random Geometries

The Karhunen-Loève Expansion is the optimal spectral expansion of a second order random process [8, 9]. It can therefore be used to characterize a random process as an infinite set of eigenvalues, eigenfunctions or eigenvectors, and associated random coefficients. The expansion uses the covariance function of the process being modeled as the kernel for a Fredholm integral equation which yields the eigenvalues and eigenvectors for the KL Expansion. Truncating the expansion allows a finite number of terms to capture most of the problem's stochastic variance.

The Karhunen-Loève Expansion can be written for a random process $g(x, \omega)$:

$$g(x, \omega) = \langle g \rangle + \sum_{k=1}^{\infty} \sqrt{\gamma_k} \phi_k(x) \xi_k(\omega), \tag{2.6}$$

where $g(x, \omega)$ is a realization through the domain of the process of interest, $\langle g \rangle$ is the average value of the process often in literature assumed to be equal to zero, γ_k, ϕ_k, and ξ_k are the eigenvalue, eigenfunction or eigenvector, and random coefficient for expansion term k, x represents dependence in the domain of the random process, and ω represents a given realization.

The eigenvalue and eigenfunction or eigenvector pairs in the KL Expansion are generated as the solution of the Fredholm integral equation:

$$\int_D cov_a(x, x') \phi_k(x') dx' = \gamma_k \phi_k(x) \tag{2.7}$$

which uses the covariance function of the random process as its kernel. If the covariance function is analytic, $\phi_k(x')$ can be solved as eigenfunctions, otherwise it is solved numerically as eigenvectors.

The eigen-spectrum is purely discrete, characterized by a countably infinite ordered set of eigenvalues and orthogonal eigenfunctions (Eq. 2.8a) which can be normalized. The expansion coefficients $\xi_k(\omega)$ are uncorrelated (Eq. 2.8b), zero-mean (Eq. 2.8c), and unit variance (Eq. 2.8d) random variables.

$$\langle \phi_{k_1} \phi_{k_2} \rangle = \delta_{k_1 k_2} \tag{2.8a}$$

$$\langle \xi_{k_1} \xi_{k_2} \rangle = \delta_{k_1 k_2} \tag{2.8b}$$

$$\langle \xi_k \rangle = 0 \tag{2.8c}$$

$$\langle \xi_k^2 \rangle = 1 \tag{2.8d}$$

The spatially random value represented by the KL expansion is reconstructed as an infinite random superposition of spatially smooth functions. In practice the expansion in Eq. 2.6 must be truncated, and from the error-minimizing property of the KL representation relatively few terms may be sufficient to capture most of the variability of the random process, depending on the correlation length λ_c relative to the size of the process domain s.

The eigenmodes are arranged such that successive eigenvalues and the contribution to the variance of successive eigenmodes decreases in magnitude. The amount of variance forfeited by truncation at term N is given by:

$$\epsilon_N^{KL} = \sqrt{\sum_{i=N+1}^{\infty} \gamma_i} \tag{2.9}$$

The exponential covariance function is a commonly encountered covariance function that is useful in the KL expansion [17–19]:

$$cov_a(x, x') = var * e^{\frac{-|x-x'|}{\lambda_c}}, \qquad var = \langle g^2 \rangle - \langle g \rangle^2, \tag{2.10}$$

where λ_c is a correlation length between points in an isotropic, weakly-stationary field. As $\lambda_c \to \infty$ the value becomes fully correlated and has no variation in the spatial domain. As $\lambda_c \to 0$ the value at spatial locations have no correlation and the value has a completely sporadic spatial structure.

Inserting the exponential covariance in Eq. 2.10 into the Fredholm equation Eq. 2.7 for a problem of domain $x, x' \in [0, s]$ produces

$$\int_0^s var * exp\left(\frac{-|x-x'|}{\lambda_c}\right)\phi_k(x')dx' = \gamma_k \phi_k(x). \tag{2.11}$$

Solution of this equation with suitable boundary conditions produces the eigenfunction and eigenvalue sets:

$$\phi_k(x) = A_k[\sin(\alpha_k x) + \lambda_c \alpha_k \cos(\alpha_k x)], \tag{2.12}$$

and:

$$\gamma_k = \frac{2 * var * \lambda_c}{\alpha_k^2 \lambda_c^2 + 1}, \tag{2.13}$$

where the values of α_k are the solutions to the transcendental equation:

$$\tan \frac{\alpha_k s}{\lambda_c} = \frac{2\alpha_k \lambda_c}{\lambda_c^2 \alpha_k^2 - 1}. \tag{2.14}$$

The normalization constant A_k is chosen such that:

$$\int_0^s \phi_k^2(x)dx = 1, \tag{2.15}$$

and becomes:

$$A_K = \sqrt{\frac{1}{\frac{s}{\lambda_c}\frac{\lambda_c^2\alpha_k^2+1}{2} + \lambda_c}}. \tag{2.16}$$

Figure 2.1 contains eigenvalue and eigenfunction examples produced using an exponential covariance function. The eigenvalues are reported as the magnitude of the ten largest eigenvalues for three different correlation lengths λ_c. In all cases the domain length s was three. Since this plot was generated from a specific problem, variance was not the same in each example. The first four eigenfunctions are plotted for the same problem (domain $s = 3$). It should be noted that as the random process becomes less spatially correlated ($\frac{\lambda_c}{s} \to 0$) the eigenvalue magnitudes fall off less quickly, meaning more eigenmodes are required for a good approximation of the process. Conversely as the problem becomes more correlated ($\frac{\lambda_c}{s} \to \infty$) the magnitudes of eigenvalues fall off much more quickly and only a few terms may be needed to capture most of the variance in the represented process.

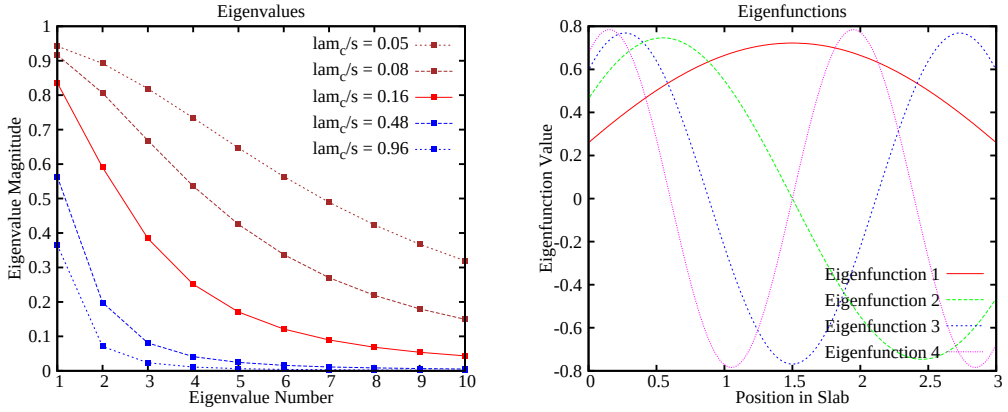

FIGURE 2.1: Example Eigenvalues and Eigenfunctions for Exponential Variance

2.4.2 Polynomial Chaos Expansion Expression of Random Coefficients

The Polynomial Chaos Expansion (PCE) was introduced by Wiener in 1938 [20] using Gaussian random variables. Other polynomial sets corresponding to other random functions were specified by Askey and Wilson in 1985 [21] and utilized by Xiu and Karniadakis in 2002 [22] to generalize Gaussian-based polynomial chaos to use with other random functions and Askey polynomial sets. The generalized PCE has been of particular interest in recent years [12, 16, 17, 19, 23–29].

For random variables $\boldsymbol{\xi} = \{\xi_1(\omega), \xi_2(\omega), \cdots, \xi_N(\omega)\}$, a random process can be viewed as a function of these random variables:

$$U(x, \omega) \equiv U(x, \boldsymbol{\xi}). \tag{2.17}$$

The random process can then be expanded using expansion coefficients u based upon an appropriate choice of orthogonal polynomials Γ_k, where k is the order of the polynomial. The expansion is then written:

$$\begin{aligned} U(x,\omega) =& u_0(x)\Gamma_0 + \sum_{i_1=1}^{\infty} u_{i_1}(x)\Gamma_1(\xi_{i_1}) \\ &+ \sum_{i_1=1}^{\infty}\sum_{i_2=1}^{i_1} u_{i_1 i_2}(x)\Gamma_2(\xi_{i_1},\xi_{i_2}) \\ &+ \sum_{i_1=1}^{\infty}\sum_{i_2=1}^{i_1}\sum_{i_3=1}^{i_2} u_{i_1 i_2 i_3}(x)\Gamma_3(\xi_{i_1},\xi_{i_2},\xi_{i_3}) + \cdots \end{aligned} \tag{2.18}$$

In practice, a limited number of random variables N must be chosen and the polynomial order of the expansion must be truncated (K). The PCE is then written as:

$$\begin{aligned} U(x,\omega) =& u_0(x)\Gamma_0 + \sum_{i_1=1}^{N} u_{i_1}(x)\Gamma_1(\xi_{i_1}) \\ &+ \sum_{i_1=1}^{N}\sum_{i_2=1}^{i_1} u_{i_1 i_2}(x)\Gamma_2(\xi_{i_1},\xi_{i_2}) + \cdots \\ &+ \sum_{i_1=1}^{N}\cdots\sum_{i_K=1}^{i_{K-1}} u_{i_1\cdots i_K}(x)\Gamma_K(\xi_{i_1},\cdots,\xi_{i_K}). \end{aligned} \tag{2.19}$$

This system contains K_t terms, where

$$K_t = \binom{N+K}{K} = \frac{(N+K)!}{N!K!}. \tag{2.20}$$

When only involving a single random variable $K_t - 1$ is the maximum polynomial order.

The expanded process can be re-written as

$$U(x,\omega) = \sum_{i=0}^{K_t} \widehat{u}_i(x)\Phi_i(\boldsymbol{\xi}), \tag{2.21}$$

where $\widehat{u}_i$ and $\Phi(\boldsymbol{\xi})$ correspond to $u_{i_1\cdots i_k}$ and $\Gamma_k(\xi_{i_1},\cdots,\xi_{i_k})$ respectively and k is an integer ranging from 1 to K. Assuming the random variables are orthonormal bases, we can write an orthogonality relationship using the inner product over the probability

space corresponding to the random function:

$$\langle \Phi_i(\xi), \Phi_j(\xi) \rangle = \int_\xi d\xi \Phi_i(\xi)\Phi_j(\xi)p(\xi) = \langle \Phi_i^2 \rangle \delta_{ij}, \tag{2.22}$$

in which the weight function $p(\xi)$ turns out to be the distribution of the random function ξ.

The stochastic Galerkin method (SGM) arises by inserting Eq. 2.21 for the response function in an equation, taking advantage of a coupling relationship of the underlying polynomials, and taking the inner product of an equation according to Eq. 2.22.

The stochastic collocation method (SCM) applies Eq. 2.22 to Eq. 2.21 and yields an expression for the flux coefficients:

$$\widehat{u}_j(x) = \frac{\langle U(x), \Phi_j(\xi) \rangle}{\langle \Phi_j^2(\xi) \rangle}, \tag{2.23}$$

which solves the coefficients through a quadrature evaluation of the numerator. We will here introduce a quadrature notation:

$$\ell^{(1)} f = \int_a^b f(\xi)p(\xi)d\xi \approx Q^{(1)} f \equiv \sum_{i=1}^{n} f\big(\xi^{(i)}\big) w^{(i)}, \tag{2.24}$$

where $\ell^{(1)}$ is an integration over one dimension, f is a function to integrate with p probability, $Q^{(1)}$ is a one-dimensional quadrature rule with n nodes, and $\xi^{(i)}$ and $w^{(i)}$ are nodes and weights in the quadrature rule. An N-dimensional quadrature rule can be expressed through tensor products:

$$\begin{aligned} \ell^{(N)} f \approx Q^{(N)} f &= \big(Q^{(1)} \otimes \cdots \otimes Q^{(1)}\big) f \\ &= \sum_{i_1=1}^{n} \cdots \sum_{i_N=1}^{n} f\big(\xi^{(i_1)}, \cdots, \xi^{(i_N)}\big) w^{(i_1)} \cdots w^{(i_N)}. \end{aligned} \tag{2.25}$$

The number of points grows in this tensor-product multi-dimensional quadrature as

$$N_Q = n^N. \tag{2.26}$$

Various quadrature rules and approaches other than isotropic, tensor-product quadrature grids will be explored in proposed work, though application of Eq. 2.25 over the integral in Eq. 2.23 is a sufficient introduction to the baseline theory which current SCM work and proposed SCM work is built upon.

Chapter 3

Monte Carlo Transport with Discrete, Random Coefficients

Here we examine transport through uncertain, discrete, and uniformly varying cross sections. We begin from the transport equation Eq. 2.1 restated for convenience:

$$\mu \frac{\partial \psi(x,\mu,\omega)}{\partial x} + \Sigma_t(x,\omega)\psi(x,\mu,\omega) = \frac{\Sigma_s(x,\omega)}{2}\int_{-1}^{1} d\mu' \psi(x,\mu',\omega), \tag{3.1a}$$

$$0 \leq x \leq s; \qquad -1 \leq \mu \leq 1 \tag{3.1b}$$

$$\psi(0,\mu,\omega) = 2, \quad \mu > 0; \qquad \psi(s,\mu,\omega) = 0, \quad \mu < 0. \tag{3.1c}$$

We define total and scattering cross sections as a function of average cross sections $\Sigma_{t,x}(x)$, a value giving magnitude to a perturbation from the average $\widehat{\Sigma}_{t,x}(x)$, and random functions which we have chosen here to be normalized and uniformly distributed $\xi_{t,x}(\omega)$:

$$\Sigma_t(x,\omega) = \langle \Sigma_t(x) \rangle + \widehat{\Sigma}_t(x)\xi_t(\omega) \tag{3.2a}$$

$$\Sigma_s(x,\omega) = \langle \Sigma_s(x) \rangle + \widehat{\Sigma}_s(x)\xi_s(\omega). \tag{3.2b}$$

Other random functions such as Gaussian, Gamma, or exponential distributions could be assumed, but our investigation has been limited to the uniform distribution.

In this chapter we investigate application of the polynomial chaos expansion to the angular particle flux with uncertainty originating in discrete, random coefficients. The stochastic Galerkin method (SGM) and stochastic collocation method (SCM) are implemented in a variety of ways. Memory and runtime scaling and convergence of the solution towards the true solution are investigated for each implementation. Planned

future work includes development of a more useful metric for convergence quantification and increased efficiency through advanced SCM grids.

3.1 The SGM Applied to the Random Transport Equation

The angular flux of the $2M$-stochastically-dimensional random transport equation with uniformly distributed random coefficients described by Eq. 3.1 and Eq. 3.2 can be represented through the polynomial chaos expansion in Eq. 2.21 using Legendre polynomials $P(\xi)$ to represent the uncertain coefficients and is written:

$$\begin{aligned}\psi(x,\mu,\boldsymbol{\xi}) &= \psi(x,\mu,\xi_{t_1}(\omega),\xi_{s_1}(\omega),\cdots\xi_{t_M}(\omega),\xi_{s_M}(\omega)) \\ &= \sum_{l_1=0}^{\infty}\sum_{m_1=0}^{\infty}\cdots\sum_{l_M=0}^{\infty}\sum_{m_M=0}^{\infty}\psi_{l_1,m_1,\ldots,l_M,m_M}(x,\mu) \\ &\qquad P_{l_1}(\xi_{t_1}(\omega))P_{m_1}(\xi_{s_1}(\omega))\ldots P_{l_M}(\xi_{t_M}(\omega))P_{m_M}(\xi_{s_M}(\omega)),\end{aligned} \tag{3.3}$$

where $\psi_{l_1,m_1,\ldots,l_M,m_M}(x,\mu)$ are the PCE expansion coefficients, also here called flux moment coefficients.

The flux moment coefficients can be solved through Eq. 2.23 which for our application with two uniformly distributed cross sections per material and involving Legendre polynomials takes the form:

$$\begin{aligned}\psi_{l_1,m_1,\ldots,l_M,m_M}(x,\mu) = a_{l_1m_1\ldots l_Mm_M}&\int_{-1}^{1}\int_{-1}^{1}\cdots\int_{-1}^{1}\int_{-1}^{1}\psi(x,\mu,\xi_{t_1},\xi_{s_1},\ldots,\xi_{t_M},\xi_{s_M}) \\ &P_{l_1}(\xi_{t_1})P_{m_1}(\xi_{s_1})\ldots P_{l_M}(\xi_{t_M})P_{m_M}(\xi_{s_M})d\xi_{t_1}d\xi_{s_1}\ldots d\xi_{t_M}d\xi_{s_M},\end{aligned} \tag{3.4}$$

where $a_{l_1m_1\ldots l_Mm_M} = \prod_{j=1}^{M}(2l_j+1)(2m_j+1)$.

To simplify notation in the following equations, we suppress the subscripts by defining $\psi(x,\mu) \equiv \psi_{l_1,m_1,\ldots,l_M,m_M}(x,\mu)$ and define a notation for flux coefficients of indices relative $\psi_{m_1-1}(x,\mu) \equiv \psi_{l_1,m_1-1,\ldots,l_M,m_M}(x,\mu)$ to that for a reference case.

We project Eq. 3.1 over the chaos functions Eq. 3.8 using our definition of uncertain cross sections in Eq. 3.2 and the following Legendre polynomial recurrence relationship:

$$\xi P_m(\xi) = \frac{m+1}{2m+1}P_{m+1}(\xi) + \frac{m}{2m+1}P_{m-1}(\xi), \tag{3.5}$$

and take the inner product of the equation with respect to the polynomials to obtain the system of SGM transport equations:

$$\mu\frac{\partial\psi(x,\mu)}{\partial x}+\langle\Sigma_{t,j}\rangle\psi(x,\mu)+\widehat{\Sigma}_{t,j}\Big[\Big(\frac{l_j+1}{2l_j+3}\Big)\psi_{l_j+1}(x,\mu)+\Big(\frac{l_j}{2l_j-1}\Big)\psi_{l_j-1}(x,\mu)\Big]=$$
$$\frac{\langle\Sigma_{s,j}\rangle}{4\pi}\phi(x)+\frac{\widehat{\Sigma}_{s,j}}{4\pi}\Big[\Big(\frac{m_j+1}{2m_j+3}\Big)\phi_{m_j+1}(x)+\Big(\frac{m_j}{2m_j-1}\Big)\phi_{m_j-1}(x)\Big],$$
$$l_1,m_1,...,l_M,m_M=0,\infty \tag{3.6}$$

where j is a designation for the material at position x.

3.2 SGM Implementations

In order to attain a PDF of the angular flux $\psi(x,\mu,\omega)$ or other derived quantities for specified locations in phase space, we must solve the system of equations represented in Eq. 3.6 for the flux moment expansion coefficients $\psi(x,\mu)$ in those locations of phase space with enough precision to sample against according to Eq. 3.3 for construction of a PDF.

Here we solve the system of coupled equations for the flux moment expansion coefficients through the tracking of only one set of particle histories in which particle weight adjustments couple flux moment coefficients. A weight array is constructed containing one entry for each flux moment coefficient. The size of the weight array depends on the SGM truncation scheme chosen. The total-order truncation scheme, which we denote "SG-1", is the one given explicitly through Eq. 2.19. The weight array produced by the SG-1 scheme is an N-dimensional simplex which contains (Eq. 2.20) $\binom{2M+K}{K}$ moment coefficients. The full-tensor-product truncation scheme, which we denote "SG-2", produces an N-dimensional hyper-cube-shaped weight array, which is convenient for array referencing and matrix operations, but requires a non-straightforward approach to Eq. **??** and may not be as computationally efficient. The polynomials of the SG-2 truncation scheme can be produced from Eq. 2.19 by allowing the max polynomial order of NK instead of K and only accepting terms of the expansion for which the subscripts of the coefficients contain K or less of the same integer. The SG-2 truncation scheme produces $K_t = N^K$ terms.

We solve flux moment coefficients using the Monte Carlo method of particle simulation taking flux tallies at each place in phase space in which we are interested in constructing a PDF of the flux. We create an array of particle weights which represents particles in the coupled equations in Eq. 3.6 and couple the particle weights in one of two ways. An

interaction-based coupling method, denoted here SG-I, adjusts weights of flux moment coefficients through a matrix inversion at scattering events associated with the average scattering cross sections $\langle \Sigma_s \rangle$ and the uncertainty in the scattering cross sections $\widehat{\Sigma}_s$ and a different matrix inversion at non-scattering events associated with the uncertainty in the total cross sections $\widehat{\Sigma}_t$. A streaming-based coupling method, denoted here SG-S, seeks a greater coupling of moments for the same number of particle histories through a similar scattering coupling scheme as in the SG-1 method but instead of coupling involving the total cross section only for non-streaming events, couples at every particle path through an eigenvalue solve involving $\langle \Sigma_t \rangle$ and $\widehat{\Sigma}_t$. This eigenvalue solve for coupling at particle streaming events requires a new eigenvalue solve for each particle distance s traveled in each material. Further discussion on the mechanics of these coupling methods can be found in [26].

The combinations of truncation methods and coupling methods produce four distinct SGM implementations: SG-1I, SG-2I, SG-1S, and SG-2S. The use of weight adjustments through the coupling of moments requires only solving one set of particle histories but is intrusive to implement and weight adjustments must be performed. In order to implement an arbitrary number of materials and thus stochastic dimensions, the array of particle weight values was collapsed into an array of rank one from which particle weight values must be retrieved from and returned to for each weight adjustment operation. Weight values needed for the same operation are rarely located contiguously in computer memory, so searching algorithms are implemented which reference values in and out of the weight array. The efficiency of these algorithms can play a significant role in the efficiency of the method. Referencing algorithms are more efficient when using the SG-2 truncation since the weight array is a hyper-cube and multiplication and modulus operations simplify a search. Referencing with the SG-1 truncation is more complicated as the weight is a simplex and involves a binary search, thus producing a greater computer time liability than the SG-2 method per moment value reference. While all implementations require larger matrix inversions or eigenvalue solves with increased dimensionality, the SG-1 schemes involve additional computational inefficiencies per moment solved: the SG-1I scheme either inverts matrices in which some of the values will not be used due to truncation or performs many smaller matrix inversions of variable size and the SG-1S scheme must solve $K - 1$ eigenvalue problems per weight adjustment since truncation has required solution of eigenvalue problems of a varying number of elements. Even with these inefficiencies per moment solved for the SG-1 truncation scheme, the SG-2 truncation scheme must solve many more moments. Ultimately the required metric for efficiency is which method converges a quantity of interest most efficiently. This is investigated in part later in this proposal and proposed as a topic of future work.

3.3 The SCM Applied to the Random Transport Equation

The stochastic collocation method (SCM) seeks to solve flux moment coefficients in Eq. 3.3 re-written:

$$\begin{aligned}\psi(x,\mu,\boldsymbol{\xi}) &= \psi(x,\mu,\xi_{t_1}(\omega),\xi_{s_1}(\omega),\cdots\xi_{t_M}(\omega),\xi_{s_M}(\omega)) \\ &= \sum_{l_1=0}^{\infty}\sum_{m_1=0}^{\infty}\cdots\sum_{l_M=0}^{\infty}\sum_{m_M=0}^{\infty}\psi_{l_1,m_1,\ldots,l_M,m_M}(x,\mu) \\ &\qquad P_{l_1}(\xi_{t_1}(\omega))P_{m_1}(\xi_{s_1}(\omega))\ldots P_{l_M}(\xi_{t_M}(\omega))P_{m_M}(\xi_{s_M}(\omega)),\end{aligned} \tag{3.7}$$

through the integral in Eq. 2.23 which becomes Eq. 3.4–or:

$$\begin{aligned}\psi_{l_1,m_1,\ldots,l_M,m_M}(x,\mu) = a_{l_1m_1\ldots l_Mm_M}&\int_{-1}^{1}\int_{-1}^{1}\cdots\int_{-1}^{1}\int_{-1}^{1}\psi(x,\mu,\xi_{t_1},\xi_{s_1},\ldots,\xi_{t_M},\xi_{s_M}) \\ &P_{l_1}(\xi_{t_1})P_{m_1}(\xi_{s_1})\ldots P_{l_M}(\xi_{t_M})P_{m_M}(\xi_{s_M})d\xi_{t_1}d\xi_{s_1}\ldots d\xi_{t_M}d\xi_{s_M},\end{aligned} \tag{3.8}$$

where $a_{l_1m_1\ldots l_Mm_M} = \prod_{j=1}^{M}(2l_j+1)(2m_j+1)$–by use of a multi-dimensional quadrature. The application of Gauss-Legendre quadrature in the tensor product form presented in Eq. 2.25 to Eq. 3.8 produces:

$$\begin{aligned}\psi_{l_1,m_1,\ldots,l_M,m_M}(x,\mu) \approx a_{l_1m_1\ldots l_Mm_M}&\sum_{k_1=1}^{K}\sum_{n_1=1}^{K}\cdots\sum_{k_M=1}^{K}\sum_{n_M=1}^{K}w_{k_1}w_{n_1}\ldots w_{k_M}w_{n_M} \\ &\psi_{k_1n_1\ldots k_Mn_M}(x,\mu)P_{l_1}(\xi_{t_1}^{k_1})P_{m_1}(\xi_{s_1}^{n_1})\ldots P_{l_M}(\xi_{t_M}^{k_M})P_{m_M}(\xi_{s_M}^{n_M}),\end{aligned} \tag{3.9}$$

where $\psi_{k_1n_1\ldots k_Mn_M}(x,\mu) \equiv \psi(x,\mu,\xi_{t_1}^{k_1},\xi_{s_1}^{n_1},\ldots,\xi_{t_M}^{k_M},\xi_{s_M}^{n_M})$ is the angular flux evaluated by fixing ξ values at quadrature points yielding cross section through Eq. 3.2 and $(\xi_{t,s}^{k,n},w_{k,n})$ are quadrature ordinates and weights. These flux coefficients are solved by evaluating independent instances in stochastic space of Eq. 3.1 and Eq. 3.2 for each set of values $k_1,n_1,\ldots,k_M,n_M$ where ξ_{t,s_m}^{k,n_m} is the quadrature ordinate corresponding to the total or scattering cross section in material m for:

$$\begin{aligned}\mu\frac{\partial\psi_{k_1n_1\ldots k_Mn_M}(x,\mu)}{\partial x} &+ [\langle\Sigma_t(x)\rangle + \widehat{\Sigma}_t(x)\xi_{t_m}^{k_m}]\psi_{k_1n_1\ldots k_Mn_M}(x,\mu) \\ &= \frac{\langle\Sigma_s(x)\rangle + \widehat{\Sigma}_s(x)\xi_{s_m}^{n_m}}{2}\int_{-1}^{1}d\mu'\psi_{k_1n_1\ldots k_Mn_M}(x,\mu'),\end{aligned} \tag{3.10}$$

still subject to the domain restrictions and boundary conditions of Eq. 3.1b and Eq. 3.1c.

3.4 SCM Implementations

In order to attain a PDF of the angular flux $\psi(x, \mu, \omega)$ or other derived quantities for specified locations in phase space, we must solve Eq. 3.10 for flux expansion coefficients at the specified locations and use them through the quadrature defined in Eq. 3.9 to attain flux moment coefficients, which can then be sampled against according to Eq. 3.7 for construction of a PDF.

Our first implementation is a straightforward Monte Carlo particle simulation in each of the instances of Eq. 3.10 to solve the flux coefficients at each of the quadrature ordinates for use in Eq. 3.9. This method is the common use of stochastic collocation and is completely non-intrusive to implement. With foresight we call this implementation of the SCM the independent stochastic collocation implementation, or I-SC.

By mimicking a technique used in the production-level, Monte-Carlo particle transport code MCNP [3], we increase the resolution of differences due to stochastic variation in tallies at different collocation points by beginning corresponding particle histories used in the solution method at each collocation point with the same random number seed. Particle history tracks diverge from one another at some point when they encounter cross sectional values that are different from one another due to the uncertainty in the cross sections. Comparing tracks at different collocation points begun with correlated random numbers removes much of the statistical variation in the problem solution such that differences in solution tallies are mostly caused by differences in uncertain parameters. This causes faster convergence of flux moments and thus any solution derived from them while maintaining a non-intrusive implementation except for the simple task of preferential random number seed setting. We call this implementation the correlated-random-number stochastic collocation, or CR-SC.

A third implementation of the SCM involves a correlated sampling technique [4, 5] in which only one set of particle histories are simulated, performing weight adjustments on an array of weights which represent the solution at each of various similar but slightly different problems. The general form for the weight adjustments is:

$$\mathbf{w_o} = \frac{p_{k_1,n_1,\ldots,k_M,n_M}}{p_{sim}} \mathbf{w_i}, \tag{3.11}$$

where $\mathbf{w_o}$ is the particle weight matrix after the adjustment for the $\psi_{k_1,n_1,\ldots,k_M,n_M}$ equation, $\mathbf{w_i}$ is the particle weight matrix before the adjustment, and $p_{k_1,n_1,\ldots,k_M,n_M}$ and p_{sim} are the event probabilities in the equation and simulated event probabilities. For more details on the specific applications of the weight adjustments see [25, 26]. Particle

history tracks are now identical at various collocation points removing statistical uncertainty and isolating uncertainty due to the uncertain inputs from the difference in the solutions at each collocation point (though enough particle histories are still needed to resolve differences in tallies due to uncertain input). Additionally, particle histories are only required to be solved one time, acquiring tallies for solutions at other collocation points using the particle weights in the weight array. This method provides computational savings which can be large over the other SCM implementations as long as weight adjustment computations remain less expensive than additional particle histories. It is, however, quite intrusive to implement and thus despite great expected savings may not be preferred for production-level codes. We call this implementation correlated-sampling stochastic collocation, or CS-SC.

We have so far only used tensor-product stochastic collocation grids, such that the number equations to be solved is K^{2M} where K is the truncation order and M is the number of materials in the problem. The CS-SC implementation is expected to be much more efficient at solving flux moments and thus derived quantities than the other implementations as long as weight adjustments are not more computationally expensive than additional sets of particle histories for a given problem. Increases in stochastic dimensionality is expected to further favor the CS-SC implementation, though it is not clear if more complicated particle physics could increase the cost of weight adjustments to the point that CS-SC loses its computational efficiency edge over CR-SC. Each implementation involving correlation is expected to be more efficient than I-SC. Future work plans to begin use of sparse SCM grids. While computational savings as a whole are expected to be great for sparse grids as compared to full-tensor SCM grids, some inefficiency per moment solved will be introduced for reasons similar to the SG-1 truncation method in which algorithms likely containing binary searches will be required to perform weight adjustments particle on weights at different collocation points.

3.5 Scaling of SGM and SCM Implementations

Computer memory requirements of the SG-1 truncation grow based on Eq. 2.19 proportionally to $\binom{2M+K}{K}$. Computer memory requirement of the SG-2 truncation and the current SCM implementations grow based on Eq. **??** proportionally to K^{2M}. Each method here suffers from the curse of dimensionality, though the SG-1 truncation method increases memory requirements more slowly with increased dimensionality than the SG-2 truncation method and current SCM implementation. This may mean that for more

stochastically complex problems the SG-1 truncation is the only practical truncation method, though even this truncation method has practical limits.

One quality of the various implementations of interest is how efficient each implementation is in terms of runtime per particle history solved for. An investigation based on this analysis quantifies the inefficiencies due to intrusive implementation described in Sections 3.2 and 3.4 such as growing matrix inversion size, multiple eigenvalue solves, and setting correlated random number seeds. A relative runtime metric is devised according to:

$$relative\ runtime = \frac{\left(\frac{runtime}{(num\ of\ histories)*(num\ of\ points)}\right)}{average\ baseline\ runtime}, \tag{3.12}$$

where the "*num of histories*" is a number of histories solved for whether through individual solution or through weight adjustments, the "*num of points*" is the number of flux moment equations or collocation points solved for, "*average baseline runtime*" is the average runtime for a particle history void of any intrusive modification for a problem, and "*runtime*" is simply the runtime of the reference problem using the implementation of interest.

In an attempt to isolate scaling with increased dimensionality in truncation order K and stochastic dimensionality as a function of number of materials M, we describe a geometry of checkered material types with identical physical specifications through a slab with an increasing number of materials in Table 3.1.

TABLE 3.1: Material Arrangements for Runtime Scaling Problems

Num of Materials	Material Arrangements									
M=1	1	1	1	1	1	1	1	1	1	1
M=2	1	2	1	2	1	2	1	2	1	2
M=3	1	2	3	1	2	3	1	2	3	1
M=4	1	2	3	4	1	2	3	4	1	2
M=5	1	2	3	4	5	1	2	3	4	5

Runtime scaling designed to quantify inefficiencies due to intrusive implementation aspects discussed in 3.2 and 3.4 according to the metric devised in Eq. 3.12 for the problem described in Table 3.1 is plotted in Figure 3.1.

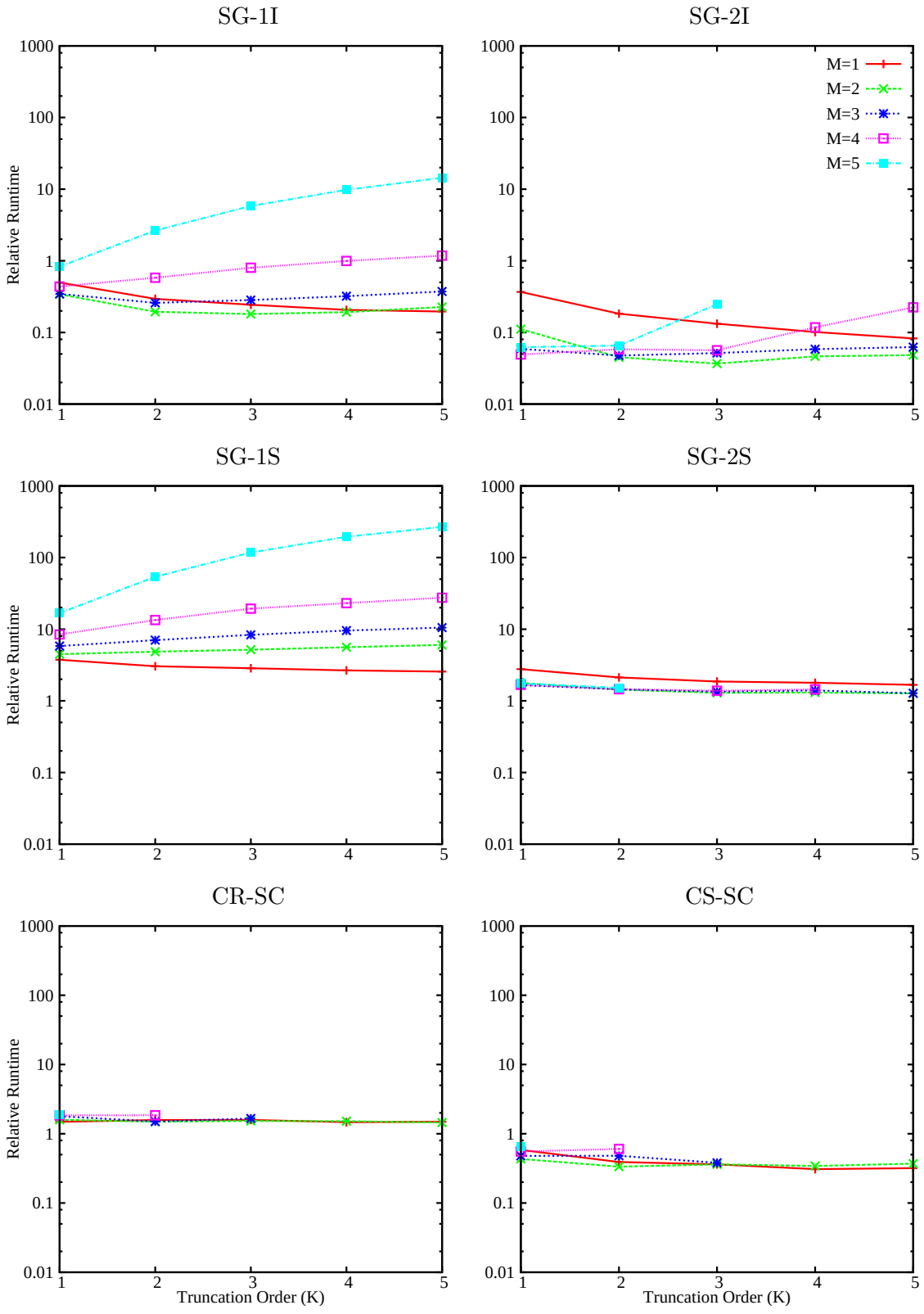

FIGURE 3.1: Runtime Scaling for Stochastic Methods

3.6 Convergence of SGM and SCM Implementations

A topic of further investigation is development of a quantity of interest derived from a PDF of flux values which would allow a convergence study of that quantity of interest with increasing number of particle histories and truncation order K for a given problem. In lieu of such a quantity we first qualitatively examine a graphical representation of a PDF of flux values generated from a reference case and with two implementations then quantitatively examine convergence rates for select flux moments.

The following plots and tables were generated based upon a slab geometry transport problem with four material chunks made up of two materials described in Table 3.2.

TABLE 3.2: Material Arrangement and Definitions for Test Problem

Material Arrangement			
1	2	2	1

Material Definitions				
Material Number	$\langle \Sigma_t \rangle$ (cm^{-1})	$\langle \Sigma_s \rangle$ (cm^{-1})	$\widehat{\Sigma}_t$ (cm^{-1})	$\widehat{\Sigma}_s$ (cm^{-1})
1	5.0	3.5	1.0	0.4
2	5.0	1.0	0.5	0.4

PDFs of transmission flux values were generated using the SG-1S and SG-2S implementations at various truncation orders K and compared against a reference solution obtained through random sampling in uncertain space. Though both methods appear to be converging, SG-2S appears to be converging more quickly as a function of truncation order K.

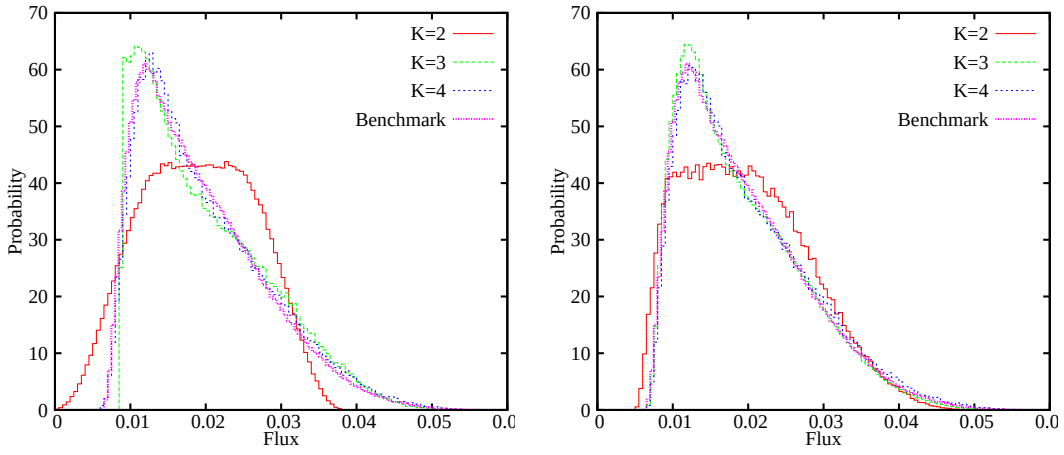

FIGURE 3.2: Transmission probability distributions for SG-1S (left) and SG-2S (right)

In order to compare the speed of convergence for various moments, a figure of merit (FOM) is introduced:

$$FOM = \frac{\bar{x}^2}{\sigma^2 T}, \tag{3.13}$$

where $\bar{x}$ is the calculated mean value for the moment, σ is the standard error of the mean, and T is the computational time spent to achieve this value.

The problem described in Table 3.2 is solved for truncation order $K = 4$ and a selection of FOM values are reported upon in Table 3.3. The benchmark Random Sampling (RS) values were attained using 1×10^7 realizations and 1×10^6 histories. All SCM and SGM implementations were solved using 1×10^8 histories each. The CS-SC implementation, with the greatest reported convergence rate for most moments, has been used to produce the reported flux moment values. Note that the letter *a* represents moments in which the standard error of the mean was greater than 10 % of the mean value and the moments have been considered not converged and the letter *b* represents a cross moment which was not solved based on SG-1 truncation.

TABLE 3.3: Efficiency Figures-of-Merit for K=4

Flux Moment		Figure of Merit						
			SCM		SGM			
l_1,m_1,l_2,m_2	ψ_{l_1,m_1,l_2,m_2}	RS	CR-SC	CS-SC	SG-1I	SG-2I	SG-1S	SG-2S
0,0,0,0	1.9E-2	1.9E+0	3.4E+1	5.2E+1	2.7E+2	1.6E+2	9.1E+1	5.0E+1
1,0,0,0	-1.2E-2	3.6E-2	1.3E+1	3.9E+1	9.6E+1	5.9E+1	5.6E+1	3.1E+1
2,0,0,0	3.0E-3	1.2E-3	6.3E-1	1.9E+1	8.9E+0	5.3E+0	2.0E+1	1.1E+1
3,0,0,0	-5.4E-4	3.1E-5	1.7E-2	7.1E+0	1.5E+0	9.1E-1	5.9E+0	3.1E+0
1,1,0,0	-2.7E-3	4.9E-4	8.3E+0	2.4E+1	1.0E+1	6.2E+0	9.9E+0	4.6E+0
2,2,0,0	1.4E-4	*a*	9.1E-1	7.1E+0	*b*	1.5E-1	*b*	5.2E-1
3,3,0,0	-5.7E-6	*a*	1.1E-1	2.2E+0	*b*	4.6E-2	*b*	7.6E-2
1,1,1,1	1.1E-4	*a*	4.8E+0	2.1E+1	*b*	*a*	*b*	3.3E-1
2,2,2,2	1.4E-7	*a*	1.3E-1	1.0E+1	*b*	*a*	*b*	*a*
3,3,3,3	1.3E-10	*a*	1.2E-3	3.3E+1	*b*	*a*	*b*	*a*
Time (s):		2.9E+6	66363	25318	1526	2558	8994	17295

a FOM values omitted due to poor statistical convergence

b Moment not calculated with this truncation method

In general all implementations produced better FOM results than the benchmark random sampling method, the SCM implementations converged the most moments, and the SGM implementations produced the best FOM values for lower-order moments. As a whole the CS-SC implementation produced the best rates of convergence, especially for the higher-order moments, though the CR-SC implementation may be the method of most interest to production-level implementation since it remains almost entirely non-intrusive and produces rates of convergence for flux moments much greater than random sampling.

Chapter 4

Monte Carlo Transport in Binary Statistical Media

Here we examine a problem in which binary Markov material mixtures are modeled according the Karhunen-Loève expansion for use in generating particle transport results. The underlying transport equation remains:

$$\mu \frac{\partial \psi(x,\mu,\omega)}{\partial x} + \Sigma_t(x,\omega)\psi(x,\mu,\omega) = \frac{\Sigma_s(x,\omega)}{2}\int_{-1}^{1} d\mu' \psi(x,\mu',\omega), \tag{4.1a}$$

$$0 \leq x \leq s; \qquad -1 \leq \mu \leq 1 \tag{4.1b}$$

$$\psi(0,\mu,\omega) = 2, \quad \mu > 0; \qquad \psi(s,\mu,\omega) = 0, \quad \mu < 0, \tag{4.1c}$$

which is a restatement of Eq. 2.1 and in which input uncertainty exists as a set of processes in physical space: the scattering ($\Sigma_s(x,\omega)$) and total ($\Sigma_t(x,\omega)$) cross sections. First we briefly describe binary Markov materials. We then present a method of generating random variable distribution probability density functions in terms of geometric properties of binary materials in a way that allows the KL expansion to be used for modeling any physical properties of the material in space. Next we present the Woodcock Monte Carlo method for effecting transport through spatially continuously varying cross sections and introduce two common approximate methods for these problem types. Finally we investigate random variable distributions and transport results, noting a limitation of the method and a possible way to minimize it. A portion of this work has been presented at a conference [30].

4.1 Binary Markov Materials

Binary Markov materials, or binary statistical mixtures, are systems in which two materials are mixed such that the average material length for each is exponentially distributed and for material m denoted λ_m. These materials are of interest in radiation transport calculations for problems involving neutron and photon transport through plasmas in fusion experiments, photon transport through clouds in weather modeling, neutron transport through water containing vapor voids in Boiling Water Nuclear Reactors, and in other applications.

A realization of these materials is commonly modeled in one-dimensional slab geometry by first randomly sampling which material touches the left boundary according to the probabilities:

$$p_1 = \frac{\lambda_1}{\lambda_1 + \lambda_2}, \qquad p_2 = \frac{\lambda_2}{\lambda_1 + \lambda_2} \tag{4.2}$$

The length of the material segment is then sampled according to an exponential distribution

$$length_m = -\frac{ln(\eta)}{\lambda_m}, \tag{4.3}$$

where η denotes a psuedo-random number. At the location which this material segment ends a material segment of the other material type begins, and is randomly sampled for length according to Eq. 4.3. This process is completed throughout the domain. The last material segment is truncated at the right boundary of the domain. This truncation causes the last segment of the material to not behave in a Markovian manner, though some investigation has suggested the effects are minimal.

Though an infinite number of unique realizations of the random process could be generated, Figure 4.1 shows three example realizations of the total cross section as a function chosen to add intuition. In this example the material with the smaller total cross section had a larger average material length. The material with the larger average material length will more often exist at the left boundary and have longer material segments in realizations. Additionally some realizations will consist of only one material or the other, although when material lengths are small compared to the domain most realizations will contain both materials.

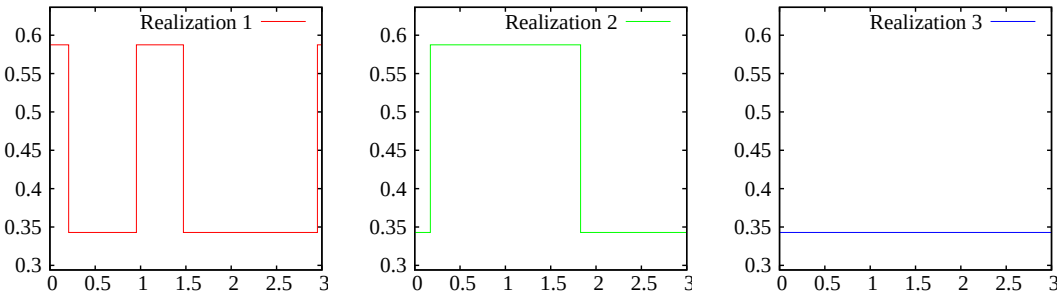

FIGURE 4.1: Example Realizations of Binary Markov Mixtures

Binary statistical media is known to be isotropically weakly-stationary such that this random process adheres to an exponential covariance function, a trait particularly desirable when using the KL expansion since eigenvalues and eigenfunctions can be analytically solved as in section 2.4.1. The correlation length used in this covariance is defined in terms of the two average material lengths as:

$$\lambda_c = \frac{\lambda_1 \lambda_2}{\lambda_1 + \lambda_2}. \tag{4.4}$$

Finally the variance of a particular type of cross section (r) for the ensemble set is found as:

$$var_r = p_1 p_2 (\Sigma_{1,r} - \Sigma_{2,r})^2. \tag{4.5}$$

Knowing that the process has an exponential covariance and knowing the process correlation length and variance allows direct use of eigenfunctions and eigenvalues solved in Eq. 2.12 and Eq. 2.13.

4.2 Construction of KL Random Variable PDFs

An appealing trait of binary statistical media for use with the KL expansion is that we know how to create realizations of the material and from a sufficiently large set of realizations we can build probability density functions for the distribution of our random variables ξ_k.

It is desirable to build PDFs from instances of ξ_k from realizations in a way that does not depend on physical material properties, and we have thus chosen a geometric material property. This allows us to use the same random distributions to model any physical property of the materials through the KL expansion. In our case this enables the modeling of scattering and absorption cross sections independently, implicitly providing the total cross section, allowing the two materials to simultaneously have different total

cross sections ($\Sigma_{t,1} \neq \Sigma_{t,2}$) and different scattering ratios ($c_1 \neq c_2$). For convenience a process was chosen which has a mean value of zero and is here labeled $\zeta_m \equiv \zeta(m(x,\omega))$ that is based only upon the relative probabilities of the materials or equivalently on the average material lengths.

Beginning by enforcing that $\langle\zeta\rangle = 0$, ζ_1 and ζ_2 are solved in terms of one another (Eq. 4.6a) and a resultantly convenient value is chosen for each (Eq. 4.6b).

$$\langle\zeta\rangle = \frac{\zeta_1 p_1 + \zeta_2 p_2}{2} = 0 \quad \Rightarrow \quad \sqrt{\frac{p_1}{p_2}}\zeta_1 = -\sqrt{\frac{p_2}{p_1}}\zeta_2 \tag{4.6a}$$

$$\zeta_1 = \sqrt{\frac{p_2}{p_1}}, \quad \zeta_2 = -\sqrt{\frac{p_1}{p_2}} \tag{4.6b}$$

As long as $p_1 \neq p_2$, one discrete value of ζ_m will have a larger magnitude than the other. We can write a piecewise definition for our new process in terms of the i-th material segment in the realization where m_i is the material index for the material in segment i:

$$\zeta(x,\omega) = \widetilde{\zeta}_i = \begin{cases} \sqrt{\frac{p_2}{p_1}}, & m_i = 1 \\ -\sqrt{\frac{p_1}{p_2}}, & m_i = 2 \end{cases}. \tag{4.7}$$

Our application of the KL expansion will be based upon this new process $\zeta(x,\omega)$.

We begin isolation of instances of the random coefficient ξ_k from Eq. 2.6 in terms of our new random process $\zeta(x,\omega)$ noting that its average value is zero as in Eq. 4.6a:

$$\zeta(x,\omega) = \sum_{k=1}^{\infty} \sqrt{\gamma_k}\phi_k(x)\xi_k(\omega). \tag{4.8}$$

We take the inner product of the equation with respect to the spatially dependent eigenfunction:

$$\int_0^s dx\phi_j(x)\zeta(x,\omega) = \int_0^s dx\phi_j(x) \sum_{k=1}^{\infty} \sqrt{\gamma_k}\phi_k(x)\xi_k(\omega). \tag{4.9}$$

The orthonormalized eigenfunctions (Eq. 2.8a and Eq. 2.15) simplify the right hand side of the equation:

$$RHS = \sum_{k=1}^{\infty} \sqrt{\gamma_k}\xi_k(\omega) \int_0^s dx\phi_j(x)\phi_k(x) = \sqrt{\gamma_j}\xi_j(\omega). \tag{4.10}$$

Re-arranging Eq. 4.9 after orthonormal simplification (Eq. 4.10) and choosing to exchange the surviving subscript j for k, we have an equation for the value of the random

variable at an eigenmode for a certain stochastic realization:

$$\xi_k(\omega) = \frac{1}{\sqrt{\gamma_k}} \int_0^s dx \phi_k(x) \zeta(x, \omega). \tag{4.11}$$

This equation may be more intuitive when written as a summation of integrals, each of which cover a part of the domain where $\zeta(x, \omega) \equiv \widetilde{\zeta}_i$ is constant. We define $I(\omega)$ to be the total number of material segments present in the domain for a realization and x_{i-1} and x_i to be the locations of the i-th material segment boundaries. Our new notation and introduced in Eq. 4.7 allows Eq. 4.11 to be written as:

$$\xi_k(\omega) = \frac{1}{\sqrt{\gamma_k}} \sum_{i=1}^{I(\omega)} \widetilde{\zeta}_i \int_{x_{i-1}}^{x_i} dx \phi_k(x). \tag{4.12}$$

This formulation allows a random variable probability density function to be numerically constructed for each eigenmode with accuracy dependent on the discretization of the PDF bins and the number of realizations over which this process is carried out.

We now seek to use the ξ_k distributions which were generated in terms of the process $\zeta(x, \omega)$ to construct realizations of various cross sections through application of Eq. 2.6. We add coefficients B_r which allow a magnitude shift in the variance of the KL expansion, enabling ξ_k values generated from $\zeta(x, \omega)$ to represent other processes, and have:

$$\Sigma_r(x, \omega) = \langle \Sigma_r \rangle + B_r \sum_{k=1}^{\infty} \sqrt{\gamma_k} \phi_k(x) \xi_k(\omega), \tag{4.13}$$

where the subscript "r" denotes whichever cross section is of interest. Before we can use Eq. 4.13 we must solve for B_r. We subtract the average cross section from both sides, take the inner product and invoke orthogonality as in Eqs. 4.8-4.12 yielding:

$$(\Sigma_r(x, \omega) - \langle \Sigma_r \rangle)^2 = B_r^2. \tag{4.14}$$

It is then apparent that

$$B_r^2 = \pm var_r. \tag{4.15}$$

Implicit in the choice of which term to make negative in Eq. 4.6b is an alignment of the sign of the ξ_k distributions with the relative magnitudes of $\Sigma_{1,r}$ and $\Sigma_{2,r}$. Specifically, the choice of $\zeta_2 < 0$ corresponds with the case that $\Sigma_{2,r} < \Sigma_{1,r}$. The other case ($\Sigma_{2,r} > \Sigma_{1,r}$) can be represented by choosing $B_r = -var_r$. In the case that $\Sigma_{1,r} = \Sigma_{2,r}$, sign is irrelevant since var_r and thus B_r is equal to zero, leaving only $\Sigma_r(x, \omega) = \langle \Sigma \rangle$.

Eq. 4.13 can now be written with B_r expressed in part as a piecewise function:

$$\Sigma_r(x,\omega) = \langle \Sigma_r \rangle + (-1)^n var_r \sum_{k=1}^{\infty} \sqrt{\gamma_k}\phi_k(x)\xi_k(\omega), n = \begin{cases} 0, \Sigma_{2,r} < \Sigma_{1,r} \\ 1, \Sigma_{2,r} \geq \Sigma_{1,r} \end{cases} . \tag{4.16}$$

Introduction of the new random process $\zeta(x,\omega)$ allows formulation of the KL expansion for use with any physical property of the binary statistical media. This allows us to construct realizations of the binary statistical media for the scattering cross section $\Sigma_s(x,\omega)$ and the absorption cross section $\Sigma_a(x,\omega)$ for the same realization ω separately from the same PDFs of ξ_k. Using this approach, the total cross section is solved through an evaluation of each of the aforementioned cross sections:

$$\Sigma_t(x,\omega) = \Sigma_s(x,\omega) + \Sigma_a(x,\omega). \tag{4.17}$$

Here we only needed to represent these two fundamental cross sections ($\Sigma_s(x,\omega)$ and $\Sigma_a(x,\omega)$) and through Eq. 4.17 the derived cross section $\Sigma_t(x,\omega)$, though this general formulation of the ξ_k distributions and subsequent evaluation using material-property specific B_r terms allows this work to be extended for more complicated physics which can involve many different cross sections of the two materials.

4.3 The Woodcock Monte Carlo Method

The traditional use of Monte Carlo particle simulation (TMC) relies upon an exponential sampling of distance to collision based upon total cross sections which are spatially discrete for portions of the domain. Each time a particle reaches an a new spatially discrete total cross section (or imposed boundary of some kind) a new sampling must be taken in order to determine the new collision and boundary distances. This makes spatially continuously varying cross sections problematic and frequently changing material geometries inefficient. Brown and Martin [31, 32] proposed a method of integrating total cross section seen by the particle as a quantity to sample against for Monte Carlo transport in spatially continuous or frequently changing materials. A more widely used approach involving rejection-sampling is called' "Woodcock sampling", "delta-tracking", or "pseudo-scattering-tracking". It was proposed for use with spatially discrete cross sections [7, 33] and rigorously proven [34, 35] in the 1960s and expanded for use with spatially continuous cross sections [6] shortly thereafter. This method has been revitalized in recent years, and is an option in several production-level Monte Carlo codes including MONK and MCBEND [36], MORET 5 [37], and Serpent 2 [38]. Schemes

involving when and how to implement WMC for greatest efficiency have been investigated [30, 37–42], and in at least one case a straightforward implementation has yielded more efficient Monte Carlo transport results than TMC [43].

The Woodcock Monte Carlo (WMC) method samples the distance to a potential, or virtual, collision based upon a the largest total cross section in the flight path of the particle. We here call that cross section the "ceiling cross section", though it has gone by at least a few other names, e.g.: "ficticious", "delta-scatterer", and "majorant" cross section. We define a ceiling cross section for a portion of the domain in 1D for our usage from x to $x + \Delta x$:

$$\Sigma_{ceil}(x, x + \Delta x) \geq max\{\Sigma_t(x + \Delta x)\}. \tag{4.18}$$

A distance to potential collision is sampled:

$$\mu x' = -\frac{ln(\eta)}{\Sigma_{ceil}(x, x + \Delta x)}, \tag{4.19}$$

where η is a psuedo-random number. The particle either streams out of the domain of $\Sigma_{ceil}(x, x + \Delta x)$ or another random number is sampled against the probability

$$P_{accept}(x + x') = \frac{\Sigma_t(x + x')}{\Sigma_{ceil}(x, x + \Delta x)}, \tag{4.20}$$

which is simply a comparison of the total cross section at the location of the potential collision to the ceiling cross section which covers a domain including the site of the potential collision. If the potential collision is rejected the particle continues streaming and a new sample for distance to potential collision is taken. If the particle interacts with the material the usual method is used to determine the fate of the particle: In our simplified physics this determination consists of selecting between particle absorption and scattering.

The WMC method can be inefficient when problems contain optically dense regions relative to the rest of the problem domain, which causes many rejected potential collision evaluations. Current implementation partially addresses this concern by choosing the smallest ceiling cross section available which is in the flight-path of a particle based upon the maximum total cross section in the cells of a superimposed grid. Another common concern with WMC is lack of sufficient information to use track length flux estimator tallies. In multi-dimensional applications this is a concern, since the method allows the exclusion of calculation of surface crossings, but such calculations in 1D are trivial.

The WMC method is the method of choice for this research when encountering spatially continuously varying cross sections, holding the advantage over deterministic solves of no discretization bias in cross section values and the advantage over TMC of being

able to effect transport through spatially non-discrete total cross section values without requiring evaluation of the a total cross section integral with respect to space.

4.4 The Atomic Mix and Levermore-Pomraning Approximations

The two most common approximations to transport through binary statistical media are the atomic mix and Levermore-Pomraning approximations. We have implemented each so that we can compare our new approximate method with existing tools seeking less required computational time than random sampling and more accurate transport results than existing approximate models.

In the atomic mix approximation, the binary materials are homogenized, creating one realization of one material where total and scattering cross sections are defined as:

$$\Sigma_t = \Sigma_{t,1} p_1 + \Sigma_{t,2} p_2 \tag{4.21a}$$

$$\Sigma_s = \Sigma_{s,1} p_1 + \Sigma_{s,2} p_2. \tag{4.21b}$$

Since the atomic mix approximation contains only one realization it does not provide a variance for quantity of interest data with respect to geometric uncertainty. It does, however, do a decent job for average quantity of interest values when the medium is highly scattering. We have implemented the atomic mix approximation.

The Levermore-Pomraning (LP) approximation was developed for finite-element transport solves of binary statistical media in which two equations, one for each material, are coupled in a way that approximates the ensemble averaged flux results. The LP equations are a modification of the random transport equation (Eq. 2.1) and can be written:

$$\mu \frac{\partial \psi^i(x,\mu)}{\partial x} + \Sigma_t^i(x)\psi^i(x,\mu) = \frac{\Sigma_s^i(x)}{2} \int_{-1}^{1} d\mu' \psi^i(x,\mu') + \frac{|\mu|}{\lambda^i}[\psi^j(x,\mu) - \psi^i(x,\mu)], \tag{4.22a}$$

$$0 \leq x \leq s; \qquad -1 \leq \mu \leq 1 \tag{4.22b}$$

$$\psi(0,\mu,\omega) = 2, \quad \mu > 0; \qquad \psi(s,\mu,\omega) = 0, \quad \mu < 0, \tag{4.22c}$$

for the material indices i=0,1; j=0,1; and j≠i [44–47]. A shortcoming of the LP equations is that they only provide an ensemble-averaged, average flux value and do not provide ensemble-averaged, higher-moment flux values. The LP approximation is exact

in purely absorbing materials though the approximation degrades as more scattering is present [44].

Not long after the development of this approximation a Monte Carlo algorithm was developed which produces the same results [48, 49]. The LP Monte Carlo algorithm adds a third distance sampling to the TMC approach which is the distance until material interface. If this is the shortest distance sampled for a flight path the particle advances that distance and continues streaming in the same direction but the material type is switched. The algorithm holds no memory of past material interfaces, but samples distance to interface at each new distance sampling. This lack of memory of interface locations is the source of approximation in the LP algorithm and allows only one ensemble realization to be solved in order to approximate ensemble averaged transport results. We have implemented the LP Monte Carlo algorithm.

For published benchmark problems some transport results are given for the atomic mix approximation and the LP approximation [46, 49]. We have implemented each of these methods so that our new method of WMC through realizations produced with the KL expansion can be compared to other approximate methods for any binary statistical mixture transport problem.

4.5 Transport Results and Method Limitation

Here we examine distributions of the random variable ξ_k used in the Karhunen-Loève representation of binary statistical media, observe a few such realizations, discuss a limitation to this approach, compare transport leakage values to approximate and benchmarks methods, and finally mention proposed work discussed further in Section 5.3 designed to alleviate the aforementioned limitation.

Figure 4.2 displays three sets of distributions of the random variable ξ_k for the first three eigenmodes of the KL expansion. The left-most plot is generated in a problem in which the correlation length is large compared to the slab thickness. In the limit $\lambda_c/s \to \infty$ every realization consists of only one material or the other. This manifests in the random variable distributions as delta functions corresponding to each case. The right-most plot is generated in a problem in which the correlation length is small compared to the slab thickness. In the limit $\lambda_c/s \to 0$ the two materials are homogenized. This is often called the atomic mix scenario and produces random variable distributions that appear to be unit Gaussians. The plot located in the center is generated in a problem existing between these two extremes in which some of the behavior of each limit is observed: both delta-function and Gaussian behavior. This is the most challenging case to solve,

as methods exists which do well in either extreme (e.g. [50] and [44]). In fact, each new method or modification to existing methods seeks to solve the problems accurately and efficiently further and further from these two extremes.

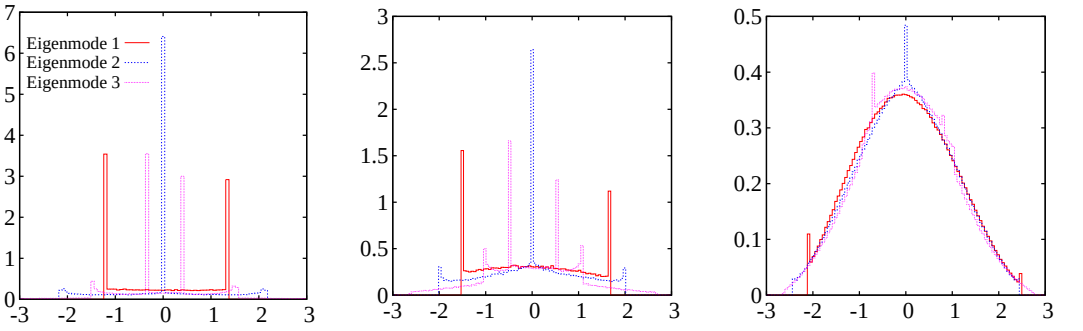

Mostly Delta, $\frac{\lambda_c}{s} = 0.57$ In Between, $\frac{\lambda_c}{s} = 0.24$ Mostly Gaussian, $\frac{\lambda_c}{s} = 0.09$

FIGURE 4.2: Regions of Random Parameter (ξ) Distributions

Should we be able to predict the distribution of the random variable with sufficient accuracy a priori we could likely use knowledge of these distributions to reduce the computational effort of the problem. Using a quadrature optimized for the distributions of the random variable in the first few eigenvalues of the KL expansion or using a transformation which can allow common quadrature to be used over these distributions [51] could allow a sufficiently accurate approximation of transport results over only N^K realizations, where N is the quadrature order chosen and K is the KL expansion truncation order chosen, reducing the need to evaluate thousands to realizations to N^K realizations. Alternatively, further modeling of the distributions in terms of delta-functions and Gaussians may allow new approaches.

Though it may become desirable to develop a method for describing these distributions a priori we have not yet developed a rigorous classification metric. Such a method for characterizing distributions would need to account for features of the distributions not yet mentioned such as significant asymmetry based upon the relative average material lengths when the two are not similar and an alternating behavior in the distribution shape of the delta-function behavior between even and odd eigenmodes. A small amount of asymmetry and the alternating behavior can be seen in Figure 4.2. Nonetheless, we have approximated limits for distributions regimes based upon the ratio λ_c/s. These regime limits are listed in Table 4.1.

TABLE 4.1: Approximate Regimes for Random Variable PDF Shapes

Region	$\lambda_c/s > 0.4$	$0.4 > \lambda_c/s > 0.1$	$0.1 > \lambda_c/s$
Shape	delta-like	both	Gaussian-like

Once random variable distributions are known, realizations can be constructed through the KL expansion. Figure 4.3 shows examples of KL reconstructed realizations using the first four eigenmodes along with realizations of the original Markov materials produced from the same material descriptions and previously presented in Figure 4.1. Individual new realizations have no direct tie to individual original realizations, but similar looking realizations were chosen from each realization generation method so that the types of created realizations could be easily visually compared.

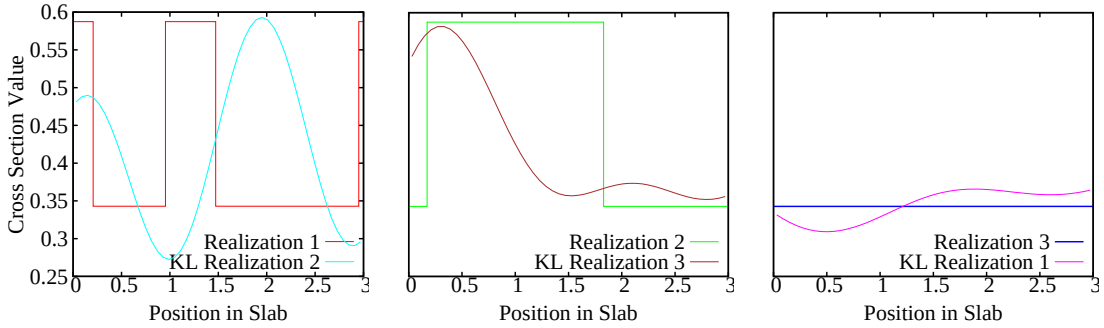

FIGURE 4.3: Example Original and Reconstructed Realizations

The primary limitation to using this method effectively with binary media is that the KL reconstructions produce negative cross section values for at least a part of the domain in many realizations for the problem class of greatest interest: more probable materials containing small cross sections mixed with less probable materials containing much larger total cross sections. The variance in the cross section is considerably larger than the mean cross section allowing dips in the reconstruction below zero while maintaining the mean and variance of the cross section in the original realizations. This unfortunate behavior when representing cross sections has been observed for such cases with large variance-to-average ratios [17].

The simplest approach to handling these negative cross sections has been to assume the cross section is zero. This approach decreases the observed variance from the reconstructions and increases the mean. Without complications such as this the KL representation of a process improves when more eigenmodes are kept, though in problems where negative cross sections are a consideration, keeping more terms of the KL expansion almost always degrades transport results since the extra variation of the cross section usually introduces more cross section negativity. For problems in which negativity is not an issue transport results through the new realizations compare roughly on par with other approximate methods and in some cases better.

Here we compare our implementation of TMC and WMC transport over original realizations, the new method using WMC with either one or four eigenmodes of the KL

reconstructions kept, and our implementation of the LP and atomic mix approximations against published benchmark values for transport over original realizations and approximate methods [46, 49]. Transport benchmark results produced by Adams, Larsen, and Pomraning were generated with a finite element (FE) solver [46]. Benchmark results produced by Brantley were generated with a Monte Carlo solver [49]. The quantities compared here are leakage values from the domain on the left and right boundaries, also known as the mean and when available the standard deviation of the particle current exiting the slab through the reflective and transmissive boundaries. The standard deviations reported represent the geometric uncertainty by assuming attainment of the exact transport solution of each realization. As a result of this assumption some additional uncertainty is introduced to these terms based upon the convergence of transport results at each realization, but since transport results have been converged to a smaller degree than the reported uncertainties this effect is expected to be minimal.

Two problem descriptions have been chosen for transport comparisons. The problems are generated with $s = 0.1$ in Table 15 of [46], here called "Adams 6.1", and the third set of values generated with $s = 10.0$ in Table 15 of [46], here called "Adams 6.3". Each of my TMC and WMC solutions was generated with 10,000 particle histories on each of 10,000 realizations. Levermore-Pomraning and Atomic Mix approximation results were generated using 1,000,000 histories. Each set of results over original realizations and published approximations produces average and standard deviation values within statistics of published values. In the "Adams 6.1" case, using only 1 eigenmode does not produce negativity in reconstructions. The approximation is rudimentary, but in this case does a pretty good job of characterizing leakage values. Using 4 eigenmodes begins to produce negativity issues in reconstructions, but for this case the effects on leakage values are minor. The "Adams 6.3" case (which has a much larger domain s than the "Adams 6.1" case but is otherwise the same) shows both the 1 eigendmode truncation and 4 eigenmode truncations falling short of converging towards the correct leakage values. For the 1 eigenmode truncation negativity issues do play a part, but the crudeness of the model is significant. The model is a much better approximation of the random process when keeping 4 eigenmodes, except that negativity issues increase in frequency and severity. As seen in this data, counting negative cross sections as zero increases the observed mean of the KL representation making the problem optically thicker and over-predicting reflection results while under-predicting transmission results.

TABLE 4.2: MC Leakage Benchmark Comparisons for Case "Adams 6.1"

Outward Particle Current on Transmissive and Reflective Boundaries				
	$\bar{x}_{reflect}$	$\sigma_{reflect}$	$\bar{x}_{trans}$	σ_{trans}
Adams-FE	0.0426	0.0985	0.9398	0.1446
Brant-TMC	0.04246		0.94005	
TMC	0.04152	0.09702	0.94123	0.14261
WMC	0.04389	0.10025	0.93773	0.14737
KL 1 Eig-WMC	0.04053	0.09716	0.94249	0.14276
KL 4 Eig-WMC	0.04066	0.10283	0.94150	0.15055
AdamsLP-FE	0.0426		0.9397	
BrantLP-TMC	0.04236		0.93985	
LP-TMC	0.04264		0.93952	
BrantAtmix-TMC	0.07455		0.90602	
Atmix-TMC	0.07457		0.90592	

TABLE 4.3: MC Leakage Benchmark Comparisons for Case "Adams 6.3"

Outward Particle Current on Transmissive and Reflective Boundaries				
	$\bar{x}_{reflect}$	$\sigma_{reflect}$	$\bar{x}_{trans}$	σ_{trans}
Adams-FE	0.4344	0.0573	0.1861	0.2134
Brant-TMC	0.43319		0.18690	
TMC	0.43308	0.05751	0.18654	0.21408
WMC	0.43297	0.05744	0.18705	0.21388
KL 1 Eig-WMC	0.46452	0.01666	0.10555	0.10976
KL 4 Eig-WMC	0.47263	0.01899	0.04054	0.8905
AdamsLP-FE	0.2910		0.1945	
BrantLP-TMC	0.28962		0.19498	
LP	0.28922		0.19461	
BrantAtmix-TMC	0.47819		0.00386	
Atmix-TMC	0.47800		0.00379	

A method for preserving the ensemble mean and possibly variance of the KL reconstructions is a topic of proposed research and is discussed in section 5.3.

Chapter 5

Proposed Research

5.1 Advanced Collocation Grids for Monte Carlo Transport with Discrete, Random Coefficients

The Chapter 3 work on this problem includes a new approach to use of polynomial chaos methods through moment coupling and correlated-sampling Monte Carlo. A better metric for determination of problem convergence is desirable. Use of advanced collocation grids may be able to greatly improve the convergence rate of the method. Research addressing these topics is proposed here.

5.1.1 Development of Metric for Solution Convergence

Current work on quantification of convergence of various SGM and SCM methods shows the appearance of convergence of the PDF of a quantity of interest and measures convergence of moments of the solution, but a functional of the response function which can be used for quantification of convergence has not been developed. Development of one or a couple of these would help answer the question of whether the additional speed of the SG-1 truncation style through evaluation of less moments of the solution in fact produces quicker convergence in a quantity of interest that is a functional of the response function particle flux. Potential quantities of interest include a norm over the PDF of flux values at a point in the slab, moments of that flux distribution, or moments of the absorption rate of the slab or a portion of the slab. A metric yielding a quantity of interest which is not expensive to calculate may be of particular importance for solution of flux coefficients through advanced SCM implementations.

5.1.2 Quadrature Rules for Use in Advanced Collocation Grids

A variety of quadrature rules are available for performing integration of Eq. 2.24, which for a tensor-product scheme is expressed in Eq. 2.25 [15, 24, 29]. Formulation of sparse cubature schemes for multi-dimensional integration are presented in following sections. Different quadrature rules can be used in each dimension, though this work plans to use the same quadrature rule in each dimension for a given problem.

The choice of quadrature rule can have significant effects on the efficiency of an SCM algorithm, especially in an adaptive algorithm, which will be discussed in further sections. Investigation for the solution particle flux PDFs in systems with spatially discrete and randomly varying cross sections has thus far assumed a uniform distribution in uncertainty space for each variable, making quadrature based on Legendre polynomials of particular interest. Thus far Gauss-Legendre quadrature has been used, which is the optimal quadrature rule for problems in which uncertainties and the solution are represented well with Legendre polynomials. Though we do not now propose assuming a different random function for the uncertainty in cross section values, in that case other quadrature rules would be more appealing; e.g. a Gaussian distribution for random variables would suggest Gauss-Hermite polynomials.

Of particular interest for adaptive methods to be discussed in the following sections are quadrature rules which are nested, meaning successive levels of quadrature re-use nodes from previous levels. This reduces the number of total solves needed for the SCM. Gauss-Legendre quadrature is not nested. Gauss-Patterson quadrature has been developed in which a first level for this rule adds $n + 1$ nodes to an existing Gauss-Legendre rule with n nodes, where the new nodes are chosen optimally with respect to the others already set. Successive levels in the same way re-use existing nodes and add $n+1$ nodes chosen optimally with respect to these [52–54]. The Gauss-Patterson quadrature rule is no longer the optimal quadrature rule for Legendre polynomials, but has the benefit of leveraging previous function evaluations in successive adaptive refinement levels. Gauss-Patterson quadrature is sometimes called Gauss-Kronrod, Kronrod-Patterson, or Gauss-Kronrod-Patterson quadrature. Genz-Keister quadrature is a version of Gauss-Hermite quadrature nested in a similar fashion as Gauss-Patterson quadrature [55]. Additional commonly used nested quadrature rules exist such as Clenshaw-Curtis quadrature and Fejér quadrature, which are both based off of Chebyshev polynomials [56–59]. The two vary only in that Clenshaw-Curtis quadrature is closed, or has nodes which exist on the boundary of the uncertain space, and Fejér quadrature is open, meaning it does not have any nodes on the boundary of the uncertain space. The Gauss quadratures we consider here are open. Chebyshev-polynomial-based quadratures are not optimal when using Legendre polynomials, but when using adaptive SCM grids they may yet converge the

solution more quickly than Legendre-polynomial-based quadratures due to the savings in the nesting of quadrature points.

For our investigation, four quadrature rules seem to be of most potential interest. Should time permit it would be valuable to implement each of them, though a subset will probably be chosen. This subset should include at least the baseline, non-nested Gauss-Legendre quadrature and at least one of the three proposed nested quadratures. At least three investigations has been done to compare two of these nested quadratures, namely Gauss-Patterson and Clenshaw-Curtis quadratures, for use in multi-dimensional integration [54, 60, 61], and another comparing performance of Gauss-Legendre quadrature to Clenshaw-Curtis [62]. These four quadrature rules are summarized in Table 5.1.

TABLE 5.1: Quadrature Rules for Use in the Sparse SCM

	Legendre-polynomial-based		Chebyshev-polynomial-based	
	Gauss-Legendre	Gauss-Patterson	Clenshaw-Curtis	Fejér
nested		x	x	x
open	x	x		x

5.1.3 Sparse and Anisotropic Collocation Grids

A definition of multi-dimensional quadrature over function f was given in Eq. 2.25 and is here in part re-stated:

$$\ell^{(N)} f \approx Q^{(N)} f = \left(Q^{(1)} \otimes \cdots \otimes Q^{(1)}\right) f. \tag{5.1}$$

We now introduce new notation which will allow this equation to represent sparse [24, 29, 63–65] and anisotropic [27, 66] collocation grids.

We define a new 1-dimensional quadrature rule which aids in construction of sparse grids:

$$\begin{aligned} \Delta_l^{(1)} &\equiv \left(Q_l^{(1)} - Q_{l-1}^{(1)}\right) f \\ Q_0^{(1)} f &\equiv 0. \end{aligned} \tag{5.2}$$

Note that for fully-non-nested collocation grids, $\sum_{i=1}^{l} \Delta_i^{(1)} f \equiv Q_l^{(l)} f$. In contrast, for nested grids $\Delta_l^{(1)}$ contains all the nodes of $Q_l^{(l)}$ but weights which are less the weight contributions of $Q_{l-1}^{(1)}$.

We also recognize that the same quadrature level is not required in each dimension, and allow $l_1, ..., l_N$ to denote quadrature levels in N stochastic dimensions. A particular combination of levels in each dimension can be expressed as a multi-index: $\mathbf{l} = (l_1, ..., l_N)$.

We can now re-write Eq. 5.1 to represent isotropic sparse collocation grids using new indices and our new quadrature rule:

$$Q_L^{(N)} f \equiv \sum_{\mathbf{l} \in \mathcal{I}(L)} \left(\Delta_{l_1}^{(1)} \otimes \cdots \otimes \Delta_{l_N}^{(1)}\right) f, \tag{5.3}$$

where L is a predetermined truncation level and $\mathcal{I}(L)$ is a truncation rule who's definition allows the freedom for various types of sparse grids. An N-dimensional grid of all valid multi-indices is commonly called a Smolyak grid, after Smoljak's initial work on sparse cubature grids [63].

We now examine three definitions for $\mathcal{I}(L)$ which directly define Smolyak grids and through Eq. 5.3 yield isotropic collocation grids:

$$\mathcal{I}_{TP}(L) = \left\{ l_n \leq L, n = 1, ..., N \right\} \tag{5.4a}$$

$$\mathcal{I}_{TD}(L) = \left\{ \sum_{n=1}^{N} l_n \leq L \right\} \tag{5.4b}$$

$$\mathcal{I}_{HC}(L) = \left\{ \prod_{n=1}^{N} l_n + 1 \leq L + 1 \right\}, \tag{5.4c}$$

where "TP" denotes the previously defined tensor-product collocation grid, "TD" represents a total-degree sparse collocation grid, and "HC" represents a hyperbolic-cross sparse collocation grid. Eq. 5.3 coupled with one of the definitions for the valid multi-index space given by Eq. 5.4 yields a unique isotropic collocation grid. The total-degree collocation scheme in general is more efficient as a function of function calls when the response function is smooth, whereas the hyperbolic-cross scheme is usually more efficient as a function of function calls when the response function is not smooth. Methods exist by which computation of these sparse collocation grids can be done in an efficient manner [67].

It may be desirable to resolve the effects of uncertainty in some dimensions more than others. This could occur when a user has reason to believe that some dimensions contribute more to the final uncertainty than others, and thus decide to put a greater importance on some for greater resolution without the same increased cost in every dimension. Anisotropic sparse grids have been developed for that purpose. As the first step in an isotropic formulation, we introduce a new multi-index $\boldsymbol{\alpha} = \alpha_1, ..., \alpha_N$ which will serve to weight the importance of each dimension. A smaller value for α_n gives higher precedence for the n dimension. We also define the 1-norm:

$$|\boldsymbol{\alpha}|_1 = \sum_{n=1}^{N} \alpha_n. \tag{5.5}$$

We now reformulate Eq. 5.4 using our new multi-index $\boldsymbol{\alpha}$:

$$\mathcal{I}_{TP}(L) = \{l_n \leq \alpha_n L, n = 1, ..., N\} \tag{5.6a}$$

$$\mathcal{I}_{TD}(L) = \{\sum_{n=1}^{N} \alpha_n l_n \leq |\boldsymbol{\alpha}|_1 L\} \tag{5.6b}$$

$$\mathcal{I}_{HC}(L) = \{\prod_{n=1}^{N} {l_n}^{\alpha_n} \leq L^{|\boldsymbol{\alpha}|_1}\},, \tag{5.6c}$$

such that Eq. 5.3 coupled with a condition from Eq. 5.6 yields an isotropic collocation grid. Anisotropic collocation grids have one primary difficulty: The user must know a priori which dimensions they wish to be resolved more than others. In many cases this information is not available. Adaptive sparse grids have been developed to handle such cases, and will discussed in the next section.

Implementation of these sparse and/or anisotropic grids is fairly straightforward based off of current work. The various formulations of cubature developed here and represented in Eq. 5.3 will solve Eq. 3.9 for values of flux moment coefficients, which are then used in Eq. 3.7 to construct PDFs of the particle flux at chosen locations in the domain. One decision to make is how to truncate the underlying PCE equations. In current work truncation of the PCE equations when using the SCM has been the tensor-product form of Eq. **??** of the same truncation order N as the SCM truncation order K. Perhaps a tensor-product or total-degree truncation (as in Eq.2.19) for the PCE equations of the same order N as the largest order in the collocation grids would be a simple and sufficient assumption, though some thought should be put into what truncation is best. Effectiveness can be measured through the convergence rates of moments and the accuracy of PDFs as in current work, or through the convergence rate of the PDF of flux as defined by the metric proposed to be developed in Section 5.1.1. What is novel is the solution method which allows correlation in solution of flux coefficients and in one case the solution of flux coefficients at many collocation points with only one underlying solve plus particle weight adjustments. The amount of work required to attain the quantity of interest, the freedom to choose a truncation for the underlying PCE equations, and the suddenly intrusive implementation of the correlated-sampling stochastic collocation will prove to make efficient implementation of adaptive grid method less than straightforward.

5.1.4 Adaptive Collocation Grids

In a classic version of adaptive cubature grids, integration space is broken up into smaller regions over which cubature integration is performed. The regions with the greatest

estimated error are broken up into smaller regions until the global error estimate is below a certain tolerance [68–71].

Other adaptive algorithms have been investigated specifically with use of the stochastic collocation method, most of them involving Lagrangian-based-SCM. Gerstner and Griebel proposed an algorithm, a version of which we propose to use for our problem, in which a Smolyak grid is built by the inclusion of successive multi-indices which resolve the greatest estimated error [13, 24, 60, 72]. A later analysis proposed anisotropic sparse collocation grids and proposed an a priori and a posteriori method for determining which dimensions to most resolve through anisotropy [66]. Another algorithm proposes a similar method to the classic adaptive cubature method in which the problem is broken up into smaller regions of integration, accept that regions with greatest error are refined through larger quadrature rules instead of smaller region discretization [73, 74]. Finally another algorithm has been proposed which grows a sparse grid by adding collocation points which a next level of refinement would add only if that region of the grid contains a high error estimate, ignoring other potential new points [75]. While earlier SCM adaptive methods refine the entire integration space anisotropically, these last two seek to only refine portions of the space and thus be more useful when problem solutions are not smooth.

At least one researcher has applied an adaptive method (Gerstner's) to the PCE-based-SCM [29]. We propose application of this algorithm but recognize that the algorithm may be optimized through modification due to specific properties of this problem: high cost of error estimate evaluation and relatively low cost of function evaluation when many points are solved at once.

The algorithm begins with a Smolyak grid constrained such that $\mathbf{l} \in \mathcal{I}$ and $\mathcal{I} = \{1, ..., 1\}$. New Smolyak grid points, defined in terms of the multi-indix $\mathbf{l}$, are candidates for inclusion in an expanded definition of $\mathcal{I}$ and are deemed "admissible" by satisfing:

$$\mathbf{l} - \mathbf{e}_j \in \mathcal{I}, \quad for 1 \leq j \leq N, l_j > 1, \tag{5.7}$$

where $\mathbf{e}_j$ is a unit vector ($(\mathbf{e}_j)_i = \delta_{ij}$). In words this states that new multi-indices are admissible if in each dimension the index one smaller than the proposed contains a current Smolyak grid point. Progressive enrichment of the collocation grid using the telescopic quadrature defined in Eq. 5.2 and soon discussed error estimates require that new Smolyak points be admissible.

We now define two subsets of multi-indices. The first, or "old", subset $\mathcal{O}$ represents all multi-indices that are part of $\mathcal{I}$ before inclusion of new multi-indices. In the first step

of the adaptive algorithm, $\mathcal{O} = \{1, ..., 1\}$. The second subset $\mathcal{A}$ consists of those multi-indices which are admissible according to Eq. 5.7 with respect to $\mathcal{O}$. At this point we use our new notation to write Eq. 5.3 in a format more convenient for adaptive collocation grids:

$$Q_{\mathcal{I}}^{(N)} f \equiv \sum_{\mathbf{l} \in \mathcal{I}} \left(\Delta_{l_1}^{(1)} \otimes \cdots \otimes \Delta_{l_N}^{(1)} \right) f, \tag{5.8}$$

where $\mathcal{I}$ can be any subset of possible multi-indices.

In order to determine which member of $\mathcal{A}$ should be next admitted into $\mathcal{O}$, each member $\mathbf{l} \in \mathcal{A}$ is assigned an estimated error $g_{\mathbf{l}}$ upon the quantity of interest resulting from its exclusion from $\mathcal{O}$. The literature presents the determination of $g_{\mathbf{l}}$ as any of several variants of

$$g_{\mathbf{l}} = \frac{\left(Q_{\mathcal{O} \cup \mathbf{l}}^{(N)} - Q_{\mathcal{O}}^{(N)} \right) f^k}{Q_{\mathcal{O}}^{(N)} f^k}, \tag{5.9}$$

where k allows calculation of any moment of the function f. This formulation is not of direct use to us, however, since we are using this cubature to determine the value of each of several flux moment coefficients which factor into our final quantity of interest. A more appropriate representation of Eq. 5.9 for our purposes may be

$$g_{\mathbf{l}} = \frac{\left(QoI\left(Q_{\mathcal{O} \cup \mathbf{l}}^{(N)}\right) - QoI\left(Q_{\mathcal{O}}^{(N)}\right) \right) f}{QoI\left(Q_{\mathcal{O}}^{(N)}\right) f}, \tag{5.10}$$

in which the quantity of interest (QoI) is based off of a metric proposed to be developed in Section 5.1.1 based off of the PDF of the flux at a point in the domain.

The estimated overall error of the computation is calculated

$$\eta \equiv \sum_{\mathbf{l} \in \mathcal{A}} g_{\mathbf{l}}. \tag{5.11}$$

The components are now established for description of the basic adaptive algorithm presented in literature.

The basic algorithm [24, 29, 72], here described in words is as follows. Initialize the old set $\mathcal{O}$ to be only the multi-index $\{\mathbf{1}\}$. Solve which multi-indices are admissible and describe them as the set $\mathcal{A}$. Solve the current solution as an evaluation of the cubature in Eq. 5.9 yielded by both the union of the old and admissible sets ($\mathcal{O} \cup \mathcal{A}$). Solve the estimated remaining error contribution for each admissible multi-index through Eq. 5.9, and the total remaining error through Eq. 5.11. As long as the total estimated error is less than the desired tolerance, begin cycling through the following sentences and previous two sentences. Select the admissible multi-index $\mathbf{l}$ with the greatest estimated error contribution $g_{\mathbf{l}}$. Remove it from the admissible set $\mathcal{A}$, add it to the old set $\mathcal{O}$,

and remove its estimated error contribution from the total estimated error. Include new qualifying multi-indices in the admissible set. Now jump back to the sentence in this description which starts with "Solve the current solution" and continue from there.

There are at least two challenges which must be overcome for implementation of the non-intrusive I-SC and CR-SC solution methods, and three for the CS-SC implementation methods. The two challenges which must be addressed for all three solution methods has roots in that our quantity of interest is not simply the cubature result, but removed by a couple additional computations. Though the adaptive nature of the grid determines which collocation points to use in solving for flux moment coefficients through a new form of the cubature formula in Eq. 3.9, it does not address what truncation to use in the underlying PCE equations of Eq. 3.7. A truncation method for these PCE equations must be decided upon. Additionally, the quantity of interest is not simply the result of the cubature, but the result of a norm applied over a PDF constructed from Eq. 3.7 which uses the result of cubature applied to each flux moment coefficient. This makes evaluation of estimated error terms much more expensive than assumed in formulation of the original algorithm. Some savings can be accomplished through pre-computing portions of the mentioned equations, and correlated sampling when constructing the PDF of the flux, but the cost of quantity of interest evaluation is still expected to be much greater than assumed in a straightforward implementation of this algorithm. Perhaps the algorithm should be modified to be more aggressive, e.g. admit two or three new multi-indices in each iteration or admit the indices which would remove a certain percentage of the estimated total error. The last challenge which is only applicable to the CS-SC solution method is that the greatest savings of this solution method come when the solution at as many collocation points as possible are solved at once. This allows great savings in the solution. From a coding implementation standpoint the growing nature of arrays inherent to this algorithm will require additional bookkeeping which may prove to be a computationally significant operation, and from an algorithmic standpoint this solution method further decreases the cost of the solution with respect to the cost of quantity of interest evaluation, suggesting that altering the algorithm to be even more aggressive may be beneficial.

The goals for this proposed research are to implement at least two quadrature rules with at least total-degree sparse grids with the option for anisotropic implementation and to implement the adaptive algorithm for the chosen quadrature rules for each of the three SCM solution methods. Convergence rates of a quantity of interest to be defined based off of the PDF of flux values at a point in the domain is then to be used for comparison of efficiency when using each approach. Approach combinations include PCE truncation choice, solution method correlation choice, stochastic collocation grid choice, number of

particle histories, and possibly other options in implementation of the advanced SCM grids.

5.2 Transport Through Nonlinear Transformations of Gaussian Random Functions

Another problem type involving random material arrangements includes cross sections distributed spatially according to continuous functions [17, 19, 51]. We plan to investigate materials with random cross sections distributed according to Gaussian or Gaussian-derived distributions. These distributions model the random cross sections through the Karhunen Loève expansion.

The random transport equation Eq. 2.1 involving a spatially random total cross section $\Sigma_t(x,\omega)$ and spatially constant scattering ratio $c \equiv \frac{\Sigma_s(x,\omega)}{\Sigma_t(x,\omega)}$ is written:

$$\mu\frac{\partial\psi(x,\mu,\omega)}{\partial x} + \Sigma_t(x,\omega)\psi(x,\mu,\omega) = \frac{c\Sigma_t(x,\omega)}{2}\int_{-1}^{1} d\mu'\psi(x,\mu',\omega), \tag{5.12a}$$

$$0 \le x \le s; \qquad -1 \le \mu \le 1 \tag{5.12b}$$

$$\psi(0,\mu,\omega) = 2, \quad \mu > 0; \qquad \psi(s,\mu,\omega) = 0, \quad \mu < 0. \tag{5.12c}$$

Uncertainty is introduced through the uncertain total cross sections $\Sigma_t(x,\omega)$ and propagates to uncertainty in the response function $\psi(x,\mu,\omega)$. The total cross section, which is a random process in physical space, can be represented using the KL expansion so that transport results can be solved using the Woodcock Monte Carlo (WMC) method on realizations of the cross section profile.

5.2.1 Transport Through Gaussian Random Processes

Utilizing the multi-index $\boldsymbol{\xi} = \{\xi_1(\omega), ..., \xi_K(\omega)\}$ which represents a selection of random values in each random distribution kept in a truncation for a realization ω, the total cross section is represented using the KL expansion (Eq. 2.6) at truncation level K:

$$\Sigma_t(x,\boldsymbol{\xi}) = \langle\Sigma_t(x)\rangle + \tilde{\Sigma}_t(x,\boldsymbol{\xi}) = \langle\Sigma_t(x)\rangle + \sum_{k=1}^{K}\sqrt{\lambda_k}\phi_k(x)\xi_k(\omega). \tag{5.13}$$

An estimation of the angular flux for realization ω is now written:

$$\psi(\boldsymbol{\xi}) = \psi(\xi_1(\omega), ..., \xi_K(\omega)) \approx \psi(\xi_1(\omega), ..., \xi_\infty(\omega)) = \psi(\omega). \tag{5.14}$$

The moments of the angular flux can then be described as the multidimensional integral:

$$\langle \psi^n \rangle \approx \int_{-\infty}^{\infty} \cdots \int_{-\infty}^{\infty} P(\boldsymbol{\xi}) \psi^n(\boldsymbol{\xi}) d\boldsymbol{\xi}. \tag{5.15}$$

Since the eigenvalues are distributed in a Gaussian manner, we know that the random variables are independent, allowing $P(\boldsymbol{\xi})$ to be described as $\Pi_{k=1}^{K} P(\xi_k)$. Eq. 5.15 then becomes

$$\langle \psi^n \rangle \approx \int_{-\infty}^{\infty} d\xi_1 P(\xi_1) \cdots \int_{-\infty}^{\infty} d\xi_K P(\xi_K) \psi^n(\boldsymbol{\xi}). \tag{5.16}$$

Since an infinite number of material arrangement realizations are possible, the multidimensional integral in Eq. 5.16 must be evaluated using some form of numerical integration. Monte Carlo sampling of realizations could be employed, but application of a cubature will converge the solution more quickly. Applying the stochastic collocation method as in Eq. 2.25 and using Guass-Hermite quadrature since the random distributions are Gaussian distributed to this multidimensional integral changes Eq. 5.16 to

$$\langle \psi^n \rangle \approx \sum_{m_1=1}^{M_1} w_{m_1} \cdots \sum_{m_K=1}^{M_K} w_{m_K} \psi^n(\mathbf{W}), \tag{5.17}$$

where $\mathbf{W}$ is a multi-index of collocation abscissas and w_{m_k} are corresponding weights. The evaluation of this integral then requires the solution of $\Pi_{k=1}^{K} M_k$ uncoupled transport equations, or if the same quadrature rule is chosen in each dimension, M^K transport equations. Sparse grids could be applied to this cubature as discussed in Section 5.1.3.

This approach can be benchmarked for a rod geometry using a solution developed by Prinja and Gonzalez-Aller [76]. Benchmark solutions for a slab geometry can be attained through Monte Carlo integration of Eq. 5.16.

5.2.2 Transport Through Gaussian-Based Random Processes

We also propose random distributions which are derived from the Gaussian distribution such as the log-normal distribution or the generalized gamma distribution. When using the normal distribution to describe the variables $\boldsymbol{\xi}$, the variable is equally likely to be negative as positive. This allows some cases of constructed cross sections to be negative for some or even all of the physical domain, an unphysical representation which provides difficulty in effecting transport, especially with a Monte Carlo solve. Other Gaussian-derived distributions contain only positive values for $\boldsymbol{\xi}$ and provide assurance of positive cross sections, however implementation for such distributions is more complex.

Here we give an example of the increased complexity for Gaussian-derived distributions. With a log-normal distribution, the total cross section can be described by

$$\Sigma_t(x, \boldsymbol{\xi}) = e^{w(x,\boldsymbol{\xi})}, \tag{5.18}$$

where $w(x, \boldsymbol{\xi})$ is a Gaussian random process with KL expansion

$$w_{KL}(x, \boldsymbol{\xi}) = \langle w(x) \rangle + \sum_{k=1}^{K} \sqrt{\lambda_k} \phi_k(x) \xi_k(\omega). \tag{5.19}$$

The log-normally distributed cross section from Eq. 5.18 then becomes

$$\Sigma_t(x, \boldsymbol{\xi}) = exp\Big(\langle w(x) \rangle + \sum_{k=1}^{K} \sqrt{\lambda_k} \phi_k(x) \xi_k(\omega) \Big). \tag{5.20}$$

A covariance function can be derived from this description for use in solving the eigenfunctions and eigenvalues involved in the KL representation. A similar approach can be used for other Gaussian-based distributions. We propose to use each of these distributions to represent random media and to apply a PCE over the particle flux so that stochastic collocation can be utilized to resolve the uncertainty resulting from these distributions, solving the transport equation in each case with a Woodcock Monte Carlo solve. Further model reduction could be achieved through advanced collocation grids.

5.2.3 Woodcock Monte Carlo Implementations and Efficiency

Part of this proposed work is to examine implementation of the WMC solve, in search of a most efficient implementation. Several researchers have devised methods for increasing the efficiency of WMC for their applications. One method allows certain regions of the domain to be treated with TMC or WMC based upon user region definitions [37]. Another defines two ceilings, one for optically thick inclusions and another for the remainder of the domain, defaulting to the lower, but imposing a boundary and switching to the higher when particles meet such inclusions [41]. A third toggles between TMC and WMC by comparing the fraction of the total local cross section to the global ceiling cross section for the energy of a particle with a user-defined value [42]. Yet another approach, which includes use of WMC over spatially continuous cross sections, allows definition of the ceiling cross section over the cells of a superimposed grid, over all material within an exclusion radius from a particle, or in user-defined regions [38].

Work to this point [30] has included use a ceiling cross section determined from use of a superimposed grid, choosing the largest total cross section between the particle and the leakage boundary in the direction of particle travel. This method can likely be

improved by a smart choice of grid-size, and allowing definition of a ceiling cross section in the direction of particle travel for a portion of the domain which does not necessarily extend to a leakage boundary. The portion of the domain chosen for the local ceiling cross section may be based upon criteria such as the gradient of ceiling cross sections for subsequent cells, the gradient of the ceiling cross section of the particle's current cell to other cells, or some sort of sampling in cells to determine an approximate or exact rejection probability based upon the number of cells chosen to be part of the local ceiling cross section domain.

A method of sampling against an optical thickness calculated as an integral of cross section in physical space may be used [31, 32] and compared against WMC implementations. This method is expected to be either analytically difficult to formulate or dependent on numerical methods for our applications such that an efficient implementation of WMC would likely be preferred.

5.3 Transport Through Binary Statistical Media - Moment Preservation

Our investigation of particle transport through Karhunen-Loève reconstructions of process realizations has produced promising results except that in the problem type of greatest interest the process for large segments of the domain is negative. This causes issues when effecting transport since negative cross sections are non-physical. We have so far handled this by assuming all negative cross sections as zero when evaluating Monte Carlo particle transport, an assumption which increases the ensemble mean and decreases the ensemble variance of the process. This handling has allowed for favorable results only when a given problem does not contain a great deal of negativity. Various games can be played in an attempt to rectify the negativity issue. We propose one in which a term is added to the KL representation which translates the reconstructed process such that the original ensemble mean of the process is restored. Should this work prove promising we may further the game through an amplitude term which restores the process variance. Should transport through mean and possibly variance preserved KL representations produce sufficiently accurate transport results, we plan to apply a quadrature over random variable distributions in order reduce the number of realizations required in the way discussed in Section 4.5. Here we describe the proposed approach to mean preservation.

We begin from the KL representation of an arbitrary cross section in Eq. 4.13, chose for notational ease this form over the more expressive Eq. 4.16, apply it to the total cross

section, and add an ensemble mean translation term $\delta\langle\Sigma_t\rangle$:

$$\Sigma_t(x,\omega) = \langle\Sigma_t\rangle + \delta\langle\Sigma_t\rangle + B_t\sum_{k=1}^{\infty}\sqrt{\gamma_k}\phi_k(x)\xi_k(\omega). \tag{5.21}$$

The ensemble averaged total cross section generated through realizations of the KL expansion $\langle\Sigma_t\rangle_{KL}$ is solved through:

$$\langle\Sigma_t\rangle_{KL} = \frac{1}{\Omega s}\sum_{\omega=1}^{\Omega}\int_0^s dx\left(\langle\Sigma_t\rangle + \delta\langle\Sigma_t\rangle + B_t\sum_{k=1}^{K}\sqrt{\gamma_k}\phi_k(x)\xi_k(\omega)\right), \tag{5.22}$$

where we have introduced Ω to represent the number of realizations chosen to approximate the ensemble of possible KL realizations.

Since at each instance a particle encounters a negative cross section it is counted as a value of zero, Eq. 5.22 does not represent the effective ensemble mean total cross section. Instead we treat sections of the domain in which the total cross section is positive and in which the total cross section is negative separately: We integrate the total cross section over positive segments and set the integral of the cross section over negative segments to zero. We represent this using the domain segment notation introduced in Eq. 4.12 and by adding a piece-wise term $\widetilde{H}_i(\omega)$ which sets the total cross section integral to zero in segments of the domain with negative total cross sections. Moving as many terms out of the integral operator as possible and determining whether a segment is positive or negative through evaluation of the total cross section at the segment mid-point, our ensemble mean total cross section equation as seen by particles is:

$$\langle\Sigma_t\rangle_{KL} = \frac{1}{\Omega s}\sum_{\omega=1}^{\Omega}\sum_{i=1}^{I(\omega)}\widetilde{H}_i(\omega)\left(\langle\Sigma_t\rangle + \delta\langle\Sigma_t\rangle + B_t\sum_{k=1}^{K}\sqrt{\gamma_k}\xi_k(\omega)\int_{x_{i-1}}^{x_i}dx\phi_k(x)\right), \tag{5.23a}$$

$$\widetilde{H}_i(\omega) = \begin{cases} 0, \langle\Sigma_t\rangle + \delta\langle\Sigma_t\rangle + B_t\sum_{k=1}^{K}\sqrt{\gamma_k}\phi_k(\frac{x_{i-1}+x_i}{2}\xi_k(\omega)) < 0 \\ 1, \langle\Sigma_t\rangle + \delta\langle\Sigma_t\rangle + B_t\sum_{k=1}^{K}\sqrt{\gamma_k}\phi_k(\frac{x_{i-1}+x_i}{2}\xi_k(\omega)) > 0 \end{cases}. \tag{5.23b}$$

Eq. 5.23 can now be used to determine the ensemble mean of the total cross section observed by the particle. This value can be compared against the actual mean of the total cross section ($\Sigma_t = p_1\Sigma_{t,1} + p_2\Sigma_{t,2}$) in order to determine the required magnitude of the translation term $\delta\langle\Sigma_t\rangle$ according to:

$$\langle\Sigma_t\rangle = \delta\langle\Sigma_t\rangle + \langle\Sigma_t\rangle_{KL} \quad \Rightarrow \quad \delta\langle\Sigma_t\rangle = \langle\Sigma_t\rangle - \langle\Sigma_t\rangle_{KL}. \tag{5.24}$$

This equation would be exact if all translation areas were of size $\delta\langle\Sigma_t\rangle s$ and would be fairly simply modified to solve for the translation term in one computation if all translation areas were rectangular. Since the KL-produced processes vary continuously, an iterative method will be needed involving Eq. 5.23 and Eq. 5.24 which solves for the mean preservation term in a way that preserves the ensemble mean to a chosen tolerance. A similar approach could be taken which restores the total cross section variance seen by the particle through the addition of a variance preservation coefficient adjacent to the B_t term in Eq. 5.21. Iteration on the mean preservation term would then be expanded to include iteration on the variance preservation coefficient as well.

It remains to be seen if preservation of the ensemble mean will correct transport results in a way that makes this method more accurate than other approximation methods. If mean preservation shows significant gains in transport result accuracy, we may next implement ensemble variance preservation. Should this method prove useful, implementation will still require answering the non-trivial question of how many eigenmodes should be used. Without consideration of negativity issues, more eigenmodes will always produce more accurate transport results, as more of the variance in the system is represented. But the presence of negative cross sections for portions of the domain increases as more eigenmodes are kept. This suggests that, even if these mean and variance preservation techniques should prove effective, there may be an optimal number of eigenmodes kept for each problem since keeping less eignmodes captures less variance in the representation and keeping more eigenmodes increases the need to manipulate the KL representation so that the mean and variance of the representation is preserved.

If moment preservation proves effective and the need to choose an optimal number of eigenmodes does not prove prohibitive, application of the PCE over particle flux so that a quadrature can be used in a stochastic collocation scheme over KL coefficients would be a natural step forward in this work. A quadrature would need to be chosen or possibly constructed which handled the unique KL coefficient PDF shapes well. Advanced SCM grids could be applied for further efficiency gains. Finally, other smoothing methods which reduce the ringing in the KL representation and thus negativities may prove useful.

Bibliography

[1] N. Metropolis and S. Ulam. The Monte Carlo method. *Journal of the American Statistical Association*, 44:335–341, 1949.

[2] E. E. Lewis and Jr. Miller, W. F. *Computational Methods of Neutron Transport*. American Nuclear Society, Inc., La Grange Park, Illinois USA, 2st edition, 1993.

[3] J. F. Briesmeister. *MCNP-A General Monte Carlo N-Particle Transport Code*. Los Alamos National Laboratory, Los Alamos, New Mexico USA, 4c edition, 2000.

[4] H. Rief. Generalized Monte Carlo perturbation algorithms for correlated sampling and a second-order Taylor series approach. *Annals of Nuclear Energy*, 11(9):455–476, 1984.

[5] H. Rief. A synopsis of Monte Carlo perturbation algorithms. *Journal of Computational Physics*, 111:33–48, 1994.

[6] L. L. Carter, E. D. Cashwell, and W. M. Taylor. Monte Carlo sampling with continuously varying cross sections along flight paths. *Nuclear Science and Engineering*, 48:403–411, 1972.

[7] E. Woodcock, T. Murphy, P. Hemmings, and T. Longworth. Techniques used in the GEM code for Monte Carlo neutronics calculations in reactors and other systems of complex geometry. In *Proceedings of the Conference on the Application of Computing Methods to Reactor Problems, ANL-7050*, Chicago, IL, May 1965. Argonne National Laboratory.

[8] M. Kac and A. Siegert. An explicit representation of a stationary Gaussian process. *Annals of Mathematical Statistics*, 18:438–442, 1947.

[9] K. Karhunen. Uber lineare methoden in der wahrscheinlichkeitsrechnung. *Annales Academiae scientiarum Fennicae, Series A. 1*, 37:3–79, 1947.

[10] Griebel M. Bungartz, H. Sparse grids. *Acta Numerical*, (13):1–123, 2004.

[11] L. Mathelin and M. Y. Hussaini. *A stochastic collocation algorithm for uncertainty analysis*. National Aeronautics and Space Administration, Washington, D. C., USA, cr-2003-212153 edition, 2003.

[12] L. Mathelin, M. Y. Hussaini, and T. A. Zang. Stochastic approaches to uncertainty quantification in CFD simulations. *Numerical Algorithms*, 38:209–236, 2005.

[13] B. Ganapathysubramanian and N. Zabaras. Sparse grid collocation schemes for stochastic natural convection problems. *Journal of Computational Physics*, (225): 652–685, 2007.

[14] M. S. Eldred and J. Burkardt. Comparison of non-intrusive polynomial chaos and stochastic collocation methods for uncertainty quantification. *American Institute of Aeronautics and Astronautics*, 2009.

[15] B. M. Adams, M. S. Ebeida, M. S. Eldred, J. D. Jakeman, L. P. Swiler, J. A. Stephens, D. M. Vigil, T. M. Wildey, W. J. Bohnhoff, K. R. Dalbey, J. P. Eddy, K. T. Hu, L. E. Bauman, and P. D. Hough. *Dakota, A Multilevel Parallel Object-Oriented Framework for Design Optimization, Parameter Estimation, Uncertainty Quantification, and Sensitivity Analysis: Version 6.1 Theory Manual*. Sandia National Laboratories, Albuquerque, New Mexico USA, 6.1 edition, 2014.

[16] S. Soga and H. S. Abdel-Khalik. Sparse approximation of POD-Galerkin generalized polynomial chaos. In *Transactions of the American Nuclear Society*, San Diego, CA, November 2012. American Nuclear Society.

[17] E. D. Fichtl. *Stochastic Methods for Uncertainty Quantification in Radiation Transport*. PhD thesis, University of New Mexico.

[18] M. M. R. Williams. The eigenfunctions of the Karhunen-Loeve integral equation for a spherical system. *Probabilistic Engineering Mechanics*, 26:202–207, 2011.

[19] E. D. Fichtl and A. K. Prinja. The stochastic collocation method for radiation transport in random media. *Journal of Quantitative Spectroscopy and Radiative Transfer*, (112):646–659, 2011.

[20] N. Wiener. The homogeneous chaos. *American Journal of Mathematics*, 60:897–936, 1938.

[21] R. Askey and J. Wilson. Some basic hypergeometric orthogonal polynomials that generalize Jacobi polynomials. *Memoirs of the American Mathematical Society*, 54: 1–55, 1985.

[22] D. Xiu and G. E. Karniadakis. The Wiener-Askey polynomial chaos for stochastic differential equations. *SIAM Journal of Scientific Computing*, 24:619–644, 2002.

[23] M. M. R. Williams. Polynomial chaos functions and neutron diffusion. *Nuclear Science and Engineering*, 155:109–118, 2007.

[24] O. P. Le Maître and O. M. Knio. *Spectral Methods for Uncertainty Quantification With Applications to Computational Fluid Dynamics*. Springer, 1st edition, 2010.

[25] B. C. Franke and A. K. Prinja. Efficient Monte Carlo solution for uncertainty propagation with stochastic collocation. In *Transactions of the American Nuclear Society*, Chicago, IL, June 2012. American Nuclear Society.

[26] B. C. Franke and A. K. Prinja. Monte Carlo solution for uncertainty propagation in particle transport with a stochastic Galerkin method. In *Proceedings of the International Conference on Mathematics and Computational Methods Applied to Nuclear Science & Engineering (M&C 2013)*, Sun Valley, ID, May 2013. American Nuclear Society.

[27] P. W. Talbot and A. K. Prinja. Sparse-grid stochastic collocation uncertainty quantification convergence for multigroup diffusion. In *Transactions of the American Nuclear Society*, Anaheim, CA, November 2014. American Nuclear Society.

[28] A. J. Olson, B. C. Franke, and A. K. Prinja. Scaling of intrusive stochastic collocation and stochastic Galerkin methods for uncertainty quantification in Monte Carlo particle transport. In *Proceedings of the Joint International Conference on Mathematics and Computation (M&C), Supercomputing in Nuclear Applications (SNA) and the Monte Carlo (MC) Method (M&C 2015)*, Nashville, TN, April 2015. American Nuclear Society.

[29] D. Ayres and M. D. Eaton. Uncertainty quantification in nuclear criticality modelling using a high dimensional model representation. *Annals of Nuclear Energy*, 80:379–402, 2015.

[30] A. J. Olson, B. C. Franke, and A. K. Prinja. Woodcock Monte Carlo transport through binary stochastic media. In *Transactions of the American Nuclear Society*, Anaheim, CA, November 2014. American Nuclear Society.

[31] F. B. Brown and W. R. Martin. Direct sampling of Monte Carlo flight paths in media with continuously varying cross-sections. In *Proceedings of Nuclear Mathematical and Computational Sciences: A Century in Review, A Century Anew (M&C 2003)*, Gatlinburg, TN, April 2003. American Nuclear Society.

[32] F. B. Brown, D. Griesheimer, and W. R. Martin. Continuously varying material properties and tallies for Monte Carlo calculations. In *Proceedings of PHYSOR 2014 - The Physics of Fuel Cycles and Advanced Nuclear Systems: Global Developments*, Chicago, IL, April 2004. American Nuclear Society.

[33] N. M. Steen. A simple method to improve the efficiency of the Σ_a/Σ_t estimator in Monte Carlo programs. In *Transactions of the American Nuclear Society*. American Nuclear Society, 1966.

[34] L. B. Miller. *Monte Carlo Analysis of Reactivity Coefficients in Fast Reactors; General Theory and Applications*. PhD thesis, University of Illinois.

[35] W. A. Coleman. Mathematical verification of a certain Monte Carlo sampling technique and applications of the technique to radiation transport problems. *Nuclear Science and Engineering*, 31:76–81, 1968.

[36] R. D. Simon, C. M. J. Baker, A. J. Bird, P. Cowan, N. Davies, G. P. Dobson, T. C. Fry, A. Kyrieleis, and P. N. Smith. MONK and MCBEND: Current status and recent developments. In *Joint International Conference on Supercomputing in Nuclear Applications and Monte Carlo 2013 (SNA + MC 2013)*, Paris, France, October 2013. American Nuclear Society.

[37] B. Forestier, J. Miss, F. Bernard, A. Dorval, O. Jacquet, and B. Verboomen. Criticality calculations on pebble-bed HTR-PROTEUS configuration as a validation for the pseudo-scattering tracking method implemented in the MORET 5 Monte Carlo code. In *International Conference on the Physics of Reactors "Nuclear Power: A Sustainable Resource"*, Interlsken, Switzerland, September 2008. American Nuclear Society.

[38] J. Leppanen. Modeling of nonuniform density distributions in the Serpent 2 Monte Carlo code. *Nuclear Science and Engineering*, 174:318–325, 2013.

[39] B. Forestier. MONTE CARLO techniques implemented in the MORET code. In *MCNEG*, Teddington, UK, March 2007. MCNEG.

[40] B. et al Forestier. Criticality calculations on realistic modelling of pebble-bed HTR-PROTEUS as a validation for the Woodcock tracking method implemented in the MORET 5 Monte Carlo code. In *International Congress on Advances in Nuclear Power Plants*, Anaheim, CA, June 2008. American Nuclear Society.

[41] J. Leppanen. *Development of a New Monte Carlo Reactor Physics Code*. PhD thesis, Helsinki University of Technology.

[42] J. Leppanen. Performance of Woodcock delta-tracking in lattice physics applications using the Serpent Monte Carlo reactor physics burnup calculation code. *Annals of Nuclear Energy*, 37:715–722, 2010.

[43] D. R. Reinert, E. A. Schneider, and S. R. F. Biegalski. Investigation of stochastic radiation transport methods in binary random heterogeneous mixtures. *Nuclear Science and Engineering*, 166:167–174, 2010.

[44] C. D. Levermore, G. C. Pomraning, D. L. Sanzo, and J. Wong. Linear transport theory in a random medium. *Journal of Mathematical Physics*, 27:2526–2536, 1986.

[45] G. C. Pomraning. *Linear Kinetic Theory and Particle Transport in Stochastic Mixtures*. World Scientific Publishing Co. Pte. Ltd., River Edge, New Jersey USA, 1st edition, 1991.

[46] M. L. Adams, E. W. Larsen, and G. C. Pomraning. Benchmark results for particle transport in a binary markov statistical medium. *Journal of Quantitative Spectroscopy and Radiative Transfer*, 42(4):253–266, 1989.

[47] B. S. Brantley and T. S. Palmer. Levermore-Pomraning model results for an interior source binary stochastic medium benchmark problem. In *Proc. International Conference on Mathematics, Computational Methods and Reactor Physics*, Saratoga Springs, NY, May 2009. American Nuclear Society.

[48] G. B. Zimmerman and M. L. Adams. Algorithms for Monte-Carlo particle transport in binary statistical mixtures. In *Transactions of the American Nuclear Society*, San Francisco, CA, November 1991. American Nuclear Society.

[49] P. S. Brantley. A benchmark comparison of Monte Carlo particle transport algorithms for binary stochastic mixtures. *Journal of Quantitative Spectroscopy and Radiative Transfer*, 112:599–618, 2011.

[50] S. D. Pautz, B. C. Franke, A. K. Prinja, and A. J. Olson. Solution of stochastic media transport problems using a numerical quadrature-based method. In *Proceedings of the International Conference on Mathematics and Computational Methods Applied to Nuclear Science and Engineering*, Sun Valley, ID, May 2013. American Nuclear Society.

[51] A. Park, M. M. R. Williams, A. K. Prinja, and M. D. Eaton. Modelling non-Gaussian uncertaintites and the Karhunen-Loève expansion within the context of polynomial chaos. *Annals of Nuclear Energy*, (76):146–165, 2015.

[52] A. S. Kronrod. *Nodes and Weights of Quadrature Formulas*. Consultants Bureau, 1965.

[53] T. N. L. Patterson. The optimum addition of points to quadrature formulae. *Mathematics of Computation*, 23:847–856, 1968.

[54] J. Burkardt, C. Webster, and G. Zhang. Slow growth for sparse grids. In *Proceedings of the SIAM Uncertainty Quantification Conference*, Savannah, GA, March-April 2014. Society for Industrial and Applied Mathematicians.

[55] A. Gentz and B. D. Keister. Fully symmetric interpolatory rules for multiple integrals over infinite regions with Gaussian weight. *Journal of Computational and Applied Mathematics*, 71:299–309, 1996.

[56] C. W. Clenshaw and A. R. Curtis. A method for numerical integration on an automatic computer. *Numerische Mathematik*, 2:197–205, 1960.

[57] L. Fejér. Mechanische quadraturen mit positiven cotesschen zahlen. *Mathematische Zeitschrift*, 37:287–309, 1933.

[58] J. Waldvogel. Fast construction of the Fejér and Clenshaw-Curtis quadrature rules. *Seminar for Applied Mathematics*, 65:682–693, 2003.

[59] A. Sommariva. Fast construction of the Fejér and Clenshaw-Curtis rules for general weight functions. *Computers & Mathematics with Applications*, 43:001–018, 2013.

[60] T. Gerstner and M. Griebel. Numerical integration using sparse grids. *Numerical Algorithms*, 18:209–232, 1998.

[61] K. Petras. On the Smolyak cubature error for analytic functions. *Advances in Computational Mathematics*, (12):71–93, 2000.

[62] L. N. Trefethen. Is Gauss quadrature better than Clenshaw-Curtis? *SIAM Review*, 50:67–87, 2008.

[63] S. A. Smoljak. Quadrature and interpolation formulas for tensor products of certain classes of functions. *Soviet Mathematics. Doklady.*, (4):240–243, 1963.

[64] V. Barthelmann, E. Novak, and K. Ritter. High dimensional polynomial interpolation on sparse grids. *Advances in Computational Mathematics*, (12):273–288, 2000.

[65] F. Nobile, R. Tempone, and C. G. Webster. A sparse grid stochastic collocation method for partial differential equations with random input data. *SIAM Journal of Numerical Analysis*, 5(46):2309–2345, 2008.

[66] F. Nobile, R. Tempone, and C. G. Webster. An anisotropic sparse grid stochastic collocation method for partial differential equations with random input data. *SIAM Journal of Numerical Analysis*, 5(46):2411–2442, 2008.

[67] K. Petras. Fast calculation of coefficients in the Smolyak algorithm. *Numerical Algorithms*, (26):93–109, 2001.

[68] P. van Dooren and L. de Ridder. An adaptive algorithm for numerical integration over an n-dimensional cube. *Journal of Computational and Applied Mathematics*, 2(3):207–217, 1976.

[69] A. C. Genz and A. A. Malik. Remarks on algorithm 006: An adaptive algorithm for numerical integration over an N-dimensional rectangular region. *Journal of Computational and Applied Mathematics*, 6(4):295–302, 1980.

[70] A. Genz. An adaptive numerical integration algorithm for simplices. *Computing in the 90's: Lecture Notes in Computer Science*, 507(4):279–285, 1991.

[71] T. Bonk. A new algorithm for multi-dimensional adaptive numerical quadrature. In *Proceedings of the Ninth GAMM-Seminar*, Kiel, Germany, January 1993. Vieweg+Teubner Verlag.

[72] T. Gerstner and M. Griebel. Dimension-adaptive tensor-product quadrature. *Computing*, 71:65–87, 2003.

[73] X. Ma and N. Zabaras. An adaptive hierarchical sparse grid collocation algorithm for the solution of stochastic differential equations. *Journal of Computational Physics*, (228):3084–3113, 2009.

[74] H. C. Elman and C. W. Miller. Stochastic collocation with kernal density estimation. *Computational Methods Applied to Mechanical Engineering*, (245-246):36–46, 2012.

[75] S. Sankaran and A. L. Marsden. A stochastic collocation method for uncertainty quantification and propagation in cardiovascular simulations. *Journal of Biomechanical Engineering*, 3(133), 2012.

[76] A. K. Prinja and Gonzalez-Aller A. Particle transport in the presence of parametric noise. *Nuclear Science and Engineering*, 124:89–96, 1996.